



Contents lists available at ScienceDirect

Remote Sensing Applications: Society and Environment

journal homepage: www.elsevier.com/locate/rsase



Impacts of the COVID-19 confinement on air quality, the Land Surface Temperature and the urban heat island in eight cities of Andalusia (Spain)

David Hidalgo García *, Julián Arco Díaz

Technical Superior School of Building Engineering, University of Granada, Technical Superior School of Building Engineering, University of Granada, Fuentenueva Campus, 18071, Granada, Spain

ARTICLE INFO

Keywords:

Urban heat island
Land surface temperature
Urban resilience
COVID- 19
Air pollution
Lockdown

ABSTRACT

The COVID-19 outbreak and ensuing global lockdown situation have generated a very negative impact on the world economy, but they have also lent us a unique opportunity to research and better grasp the impacts of human activity on environmental pollution and urban climates. Such studies will be of vital importance for decision-making on measures needed to mitigate the effects of climate change in urban areas, in order to turn them into resilient environments. This study looks at eight cities in the region of Andalusia (southern Spain) to comprehensively assess their environmental quality with parameters (Pm_{10} , SO_2 , NO_2 , Co and O_3) obtained from meteorological stations. The aim was to determine how these parameters affect the Land Surface Temperature (LST) and the Surface Urban Heat Island (SUHI), on the basis of Sentinel 3 satellite thermal images. Knowing to what extent improved air quality can reduce the LST and SUHI of cities will be essential in the context of future environmental studies on which to base sustainable decisions. The geographic situation of cities in the Mediterranean Sea basin, highly vulnerable to climate change, and the high pollution rates and high daily temperature variations of these urban areas make them particularly attractive for analyses of this sort. During the confinement period, average reductions of some environmental pollutants were achieved: SO_2 (-33.5%), Pm_{10} (-38.3%), NO_2 (-44.0%) and Co (-26.5%). However, the environmental variable O_3 underwent an average growth of 5.9%. The LST showed an average reduction of -4.6 °C (-19.3%), while the SUHI decreased by 1.02 °C (-59.8%). These values exhibit high spatio-temporal variations between day and night, and between inland and coastal cities.

1. Introduction

In December 2019, the outbreak of a new disease associated with the severe acute respiratory syndrome Coronavirus 2 (SARS-CoV-2) was reported for the first time in the city of Wuhan (China). On January 30, 2020, after having recorded 7711 confirmed cases and 12167 suspected cases (WHO, 2020), the World Health Organization (WHO) declared it an international public health emergency entailing a high risk for the vulnerable health care system (Mandal and Pal, 2020; Sohrabi et al., 2020). Faced with this situation, most countries of the world imposed or recommended some sort of “lockdown” for their inhabitants, which led to a sudden paralysis of the tourism, industry and transport sectors, affecting the global world economy (He et al., 2020; Ray et al., 2020; Huang et al., 2021). In Spain, the mandatory home confinement decreed by the Government lasted from March 15 to April 28—a total of 48

* Corresponding author.

E-mail addresses: dhidalgo@ugr.es (D. Hidalgo García), juliannn@ugr.es (J. Arco Díaz).

days. Numerous studies report that this circumstance caused a substantial reduction in the adverse environmental effects of usual activities (Ghosh et al., 2020; He et al., 2020; Maithani et al., 2020; Mandal and Pal, 2020; Ray et al., 2020; Ali et al., 2021; Huang et al., 2021; Toro et al., 2021).

Although the widespread blockade meant significantly negative impacts on the global economy (Ray et al., 2020; Huang et al., 2021), it stood as an excellent opportunity to study possible variations in air pollution emissions and link them to the environmental temperature and the climate alteration known as Surface Urban Heat Island. Some studies report on the relationship between UHI and environmental pollution due to a mixture of turbulence and radiation transfer processes (Sabatino et al., 2020; Schaefer et al., 2021), accentuating the importance of studying these elements together. Although the environmental temperature and the LST are different, numerous studies confirm that they are correlated (Avda and Jovanovska, 2016; Srivastava et al., 2009), mostly through the use of satellite images.

In recent months, various studies have reported improvements in the environmental quality of cities due to reductions in emissions and pollution (Ghosh et al., 2020; Mandal and Pal, 2020; Pani et al., 2020; Ali et al., 2021; Das et al., 2021; Jiang et al., 2021; Nakajima et al., 2021; Srivastava et al., 2021; Toro et al., 2021). Accordingly, NO_2 and carbon emissions in China were reduced by between 25% and 30% (Lauri, 2020; Mandal and Pal, 2020). The European Space Agency (ESA) documented a noteworthy reduction in nitrous oxide emissions in the Po River valley (northern Italy), based on environmental measurements made by the Sentinel 5P satellite under the Copernicus program (Mandal and Pal, 2020). In New Delhi (India), the levels of $\text{PM}_{2.5}$ and Co were reduced by 71% (Mitra et al., 2020); in Calcutta, environmental pollution was reduced by 80% (Das et al., 2021). The Dwarka River basin located in eastern India showed a 74% reduction in PM_{10} levels after 18 days of lockdown (Mandal and Pal, 2020). The city of Dehradun (India) witnessed a 46% reduction in the NO_2 indices, while the environmental quality index improved by 27% (Maithani et al., 2020).

Despite research studies that positively link environmental pollution with an increase in LST and the intensity of SUHI (Schwarz et al., 2011; Li et al., 2011; Logan et al., 2020; Venter et al., 2020), variations due to the lockdown situation caused by the pandemic have hardly come to light in scientific publications. According to recent reports, decreases in the LST range from 0.13 °C for the city of Osaka (Nakajima et al., 2021); 0.49 °C in Tokyo (Fujibe, 2020); 1 °C in Montreal (Canada) (Teufel et al., 2021); and 3 to 5 °C in the Dwarka River basin (Mandal and Pal, 2020), alongside values between 5 and 8 °C in the San Francisco Bay area (Potter and Alexander, 2021). A study involving the cities of Mumbai, Delhi, Kolkata, and Chennai (India) reports a drop in the average intensity of the SUHI during the lockdown period amounting to 19.2% (Ghosh et al., 2020). Similar values were obtained for nine cities in Pakistan, where average SUHI reductions of 19.5% were reported for five megacities and 8.7% in four major cities (Ali et al., 2021). A UHI reduction of -0.3 to -1.4 °C was found for Montreal (Canada) using high-resolution simulations (Teufel et al., 2021).

Given that greenhouse gases such as SO_2 , NO_2 , Co and PM_{10} are considered a predominant cause of climate change and of disease (Andersson and Nässén, 2016; Bashir et al., 2020; Pani et al., 2020), the study of their concentrations in exceptional situations—as in the wake of COVID-19—is of vital importance. These studies help urban planners and public administrations to adopt pollutant mitigation measures, contributing to a map of cities that are resilient to climate change in terms of LST and SUHI phenomena.

The UHI generates a series of environmental, climatic and socioeconomic problems with negative implications for the quality of life in urban areas (Dwivedi and Mohan, 2018; Macintyre et al., 2018; Yang et al., 2020a), water and air quality (Feizizadeh and Blaschke, 2013), biodiversity (Čeplová et al., 2017), the energy balance (Arnfield, 2003), the regional climate (Sarrat et al., 2006), the cost of energy (Santamouris, 2020) and even mortality (Arbuthnott and Hajat, 2017). Therefore, gaining exhaustive knowledge about this phenomenon, its properties, and the factors that intensify it constitute an increasingly vital challenge for urban populations.

The methodologies most commonly applied to determine the UHI are: mobile transects, fixed temperature probes, and comparison between meteorological stations. To determine the SUHI and since the 1990s, remote sensing is most common. The latter makes large-scale urban LST and SUHI studies possible (Song et al., 2018) with reference to satellite images having thermal infrared remote sensors (TIRS). Studies involving these systems constitute an important field of research, with extensive output (Wang and Ouyang, 2017; Yao et al., 2018; Guo et al., 2020; Hu et al., 2020; Shafizadeh-Moghadam et al., 2020; Yang et al., 2020a).

At present, many satellites allow us to obtain thermal images of the earth's surface: Goes (1978), MODIS (1999), NOAA AVHRR (1999), Landsat 8 (2013), Sentinel 3 (2018), and Ecostress (2018). The latter three are the newest, having been launched recently and featuring novel high-resolution TIRS sensors. Landsat 8 enables one to obtain LST estimates every 16 days at a resolution of 100 m, thanks to its thermal bands 10 and 11. By means of this satellite, the SUHI of multiple cities has been determined: Bangladesh (India) (Roy et al., 2020), Changchun (China) (Yang et al., 2020a), Barcelona (Spain) (Lemus-Canovas et al., 2020), Shanghai (China) (Li et al., 2011), the Beijing Olympic area (China) (Hu et al., 2020), Xiamen city (China) (Hua et al., 2020), Fuzhou (China) (Du et al., 2020), Lyon (France) (Diallo et al., 2015), or Krakow (Poland) (Walawender et al., 2014).

The Ecostress thermal sensor is installed on the International Space Station and has six thermal infrared spectral bands with a resolution of 60 m, providing for temperature estimates every four days. Its use for determining the LST is documented through studies of cities in the United States (Coleman et al., 2020; Xue et al., 2020). The latest product is the constellation Sentinel 3, made up of satellites 3A, 3B and 3C. The first two were released in February 2016 and April 2018, respectively, while the Sentinel 3C does not yet have a release date. The Sentinels have 3 TIRS channels—bands 7, 8 and 9—that provide LST estimates every day and at a resolution of 1000 m. Their use is documented in SUHI studies on the cities of Daman (India) and Huazhaizi (China) (Yang et al., 2020b), Oklahoma City (USA), Dahra (Senegal) (Sobrino et al., 2016) and Granada (Spain) (Hidalgo and Arco, 2021). Although using Sentinel 3 to determine LST and SUHI is not as common as Landsat 8 and ECOSTRESS, it offers an important advantage in this type of study. Namely, while the latter orbit only once daily over each point on the planet, respectively every 16 and 4 days, Sentinel 3 does so twice, once during the day and then again at night.

In addition, Sentinel 3 determines the LST directly by downloading level 2 satellite products, whereas the LST obtained by Landsat 8 and ECOSTRESS requires using algorithms to transform atmospheric spectral radiance into brightness temperature. To this end, it is necessary to precisely know the emissivity of the soil and the humidity of the atmosphere. Although these algorithms have been widely studied, their use can prove to be a cumbersome process, sometimes giving erroneous or misleading results (Li et al., 2011; Yang et al., 2020).

Recent estimates (Ward et al., 2016; Cramer et al., 2018) affirm that the temperatures of the areas located in the Mediterranean Sea basin are increasing at a faster rate than those of the rest of the planet. In other words, this setting is considered prone to climate impacts. It is therefore essential to probe new methodologies and systems able to discern —quickly but also accurately— the spatial-temporal variability of the LST and the SUHI of Mediterranean urban areas in view of environmental and pollution conditions. The exceptional situation of home confinement generated by COVID-19 made for a very interesting research scenario.

The objective of this study is to determine how the context of home confinement established by Spain's central Government translates into a variability of environmental pollution, LST and SUHI in eight Andalusian cities (southern Spain), according to Sentinel 3 satellite data. The location of the cities, in the Mediterranean Sea basin, adds emphasis to the endeavour. By means of statistical procedures, correlations between the data obtained and relationships between/among variables could be determined, ensuring the validity of results. The Data Panel technique is presented as a novel element when applied to research on SUHI, as it allows for the incorporation of more data and variables by admitting the individual effects of a certain zone when deriving the global results. It furthermore allowed us to include the spatial residual values of our results, and eliminate the common problem of collinearity between variables. These elements are often neglected by traditional analytical methods and can interfere with the accuracy and thoroughness of results. As far as we know, our research is the first of its kind to be conducted on a Spanish city.

Therefore, the questions that we propose to answer are as follows: 1. Can a situation of home confinement reduce the levels of environmental contamination? 2. What influence could the reduction of pollutants in the atmosphere have on the LST and SUHI of the cities studied? 3. Would this influence be the same for daytime and nighttime LST and SUHI? 4. Can the results be extrapolated to other settings or prove useful for future urban planning?

The progress made through this research contributes to an open-source work environment that allows environmental scientists to assess the influence of environmental pollutants on LST and SUHI. Taking into account the geographic, climatological and pollution characteristics of cities, our findings provide a basis of empirical evidence that complements the results obtained in previous studies. Altogether, such research efforts will aid future decision-making by urban planners and public administrations regarding measures needed to mitigate the effects of increased LST and SUHI, aspiring toward environments resilient to climate change.

2. Materials and methods

2.1. Study area and data source

The area under study comprises the eight provincial capitals of the region of Andalusia, located in southern Spain (Fig. 1). Its characteristics in terms of population, surface, climate, rainfall, altitude and UTM coordinates are found in Table 1.

According to Spain's National Institute of Statistics (NIS), Andalusia covers an area of 87,268 km² and has a population of 8,427,325, being the second largest region of Spain as well as the most highly populated one. The region features somewhat diverse background climates. According to the Koppen-Geiger climate classification, the cities of Cadiz and Huelva share a Mediterranean Oceanic climate (Csb), the cities of Sevilla, Malaga, Cordoba and Jaen feature a Mediterranean climate (Csa), and Granada and Almería have a cold semi-arid climate (Bsk). These typologies imply mild, humid winters and hot, dry summers (de Castro et al., 2007). The region is bordered by mountains to the north, while the Mediterranean Sea lies to the south. This circumstance makes the sea and land breezes strongly impact coastal cities. The average altitude is 503 m above sea level; the annual average temperature fluctuates between 11 °C in January and 26.4 °C in July, with a minimum in winter of -3 °C and extremes in summer of up to 44.5 °C. The approximate number of hours of sunshine per year ranges between 2800 and 3200, giving an average between 7.67 and 8.76 h of sunshine per day, depending on the area within the Andalusian region.

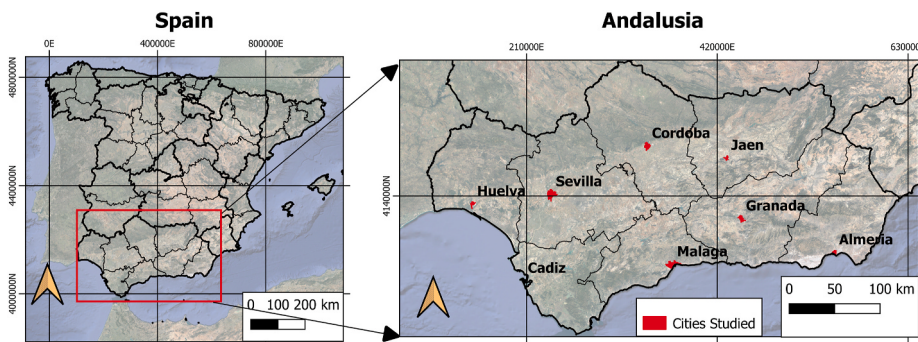


Fig. 1. Study area of Andalusia, Spain.

Table 1

Characteristics of the cities of Andalusia.

Geographic information	Sevilla	Cordoba	Jaen	Granada	Huelva	Cadiz	Malaga	Almeria
Downtown location	37.375N, -6.025W	37.891N, -4.819W	37.780N, -3.831W	37.111N, -3.362W	37.270N, -6.974W	36.516N, -6.317W	36.765N, -4.564W	36.841N, -2.492W
Climate Zone	Csa	Csa	Csa	Csa y Bsk	Csb	Csb	Csa	Bsk
Mean annual T. (°C)	18.6	17.8	16.9	15.5	17.8	17.9	18.4	17.9
Average annual rainfall (mm)	576	612	552	450	467	597	520	228
Total area (km ²)	140.8	1253	424	88.8	151.3	13.3	398	296.2
Total urban area (km ²)	68.69	31.35	9.43	21.78	14.87	7.34	58.6	14.95
Population in 2019 (hab)	688592	325701	112999	232462	143663	116027	574654	198533
Urban mean elevation (masl)	11	106	570	680	24	13	8	16

2.2. Methodology

The methodology carried out to develop this research is described in Fig. 2.

In order to validate the LST data of the eight cities, based on Sentinel 3A and 3B images, the method of comparison with the environmental temperature data (recorded 1–2 m from the ground) from the AEMET network of meteorological stations was followed. The two temperatures are not the same, but their comparison has been used as a validation system in numerous scientific studies (Srivastava et al., 2009; Gallo et al., 2011; Avdan and Jovanovska, 2016; Rongali et al., 2018). The environmental pollution values (PM_{10} , SO_2 , NO_2 , CO and O_3) were obtained from the US-EPA Environmental Monitoring Network. To derive concise results according to geographic characteristics, the cities were classified as either inland or coastal.

The Data Panel statistical method was used for data analysis. Unlike more traditional methods of analysis, it admits even the individual effects of each city in the overall result, while eliminating the problem of collinearity between variables. This allowed us to reflect possible variations in the conditions of each city contemplated in the final results, making it a unique and powerful approach. It has been validated by studies (Chen et al., 2011; Alcock et al., 2015; Fang and Tian, 2020) similar to ours, including time series studies of multiple cities or areas, as well as quantitative variables when the conditions may vary among the cities analyzed.

2.3. Sentinel 3 images

Sentinel 3 satellites are equipped with the high-resolution scanning instrument Land Surface Temperature Radiometer, enabling LSTs of the Earth's surface to be obtained. The images consist of six spectral bands with a resolution of 500 m (bands S1 to S6) and

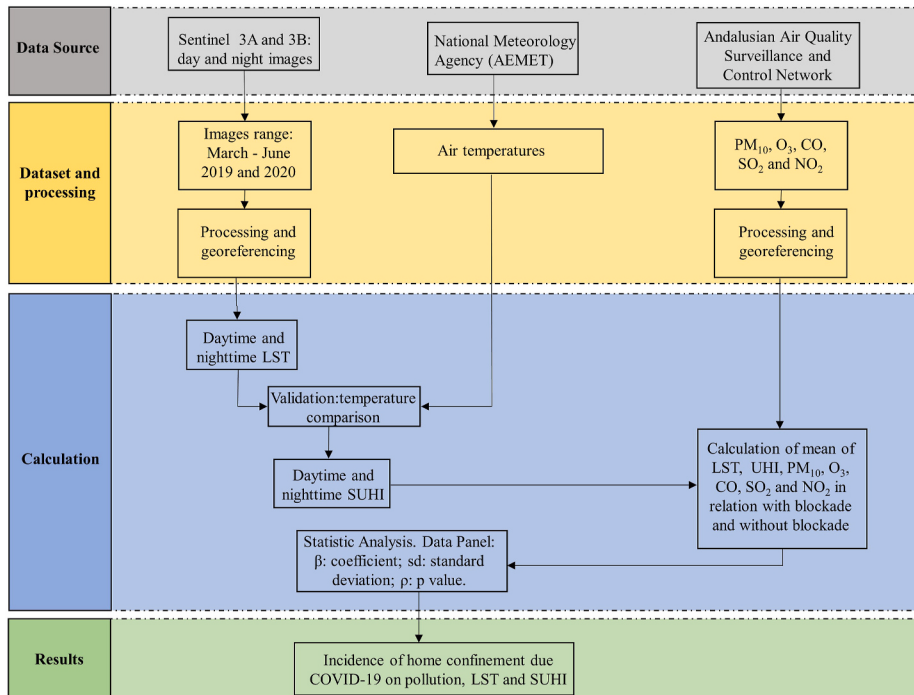


Fig. 2. Investigation methodology.

three thermal bands that make it possible to determine the LST (bands S7, S8 and S9), having a resolution of 1000 m. The Sentinel 3 level 2 thermal products directly and automatically include the LST together with associated parameters: e.g. the normalized difference vegetation index (NDVI), type of vegetation (Biome), vegetal fraction (PV) and normalized difference building index (NDBI). Andalusia lies below the route of the Sentinel 3A and 3B satellites. The usual time of passage of the first over the region during the day is between 9:00 and 11:00 h, while the passage of the second is at night between 20:00 and 22:00. The images chosen for the study correspond to twenty days distributed evenly between the months of March and June of the year 2020. Of these, five images correspond to days on which there was no home confinement, the other five to lockdown days. In order to corroborate the possible variations of LST and UHI during the confinement and non-confinement periods within the year 2020, the images of the same days in the year 2019 were also downloaded.

Thus, throughout this time interval, a total of 40 images were used, 20 corresponding to Sentinel 3A and 20 to Sentinel 3B ([Tables 2 and 3](#)). All of them have a cloudiness index of less than 15%, thereby ensuring accuracy when obtaining the LST and subsequently calculating the UHI. The images were acquired from the European Space Agency (ESA) Copernicus Open Access Hub for level 2.

After downloading the images, the resolutions of bands 8 and 9 were georeferenced using the ETRS89/UTM Zone 30N projection system. Both reclassification and atmospheric correction were carried out using the Toolbox (S3TBX) under the open-source software environment Sentinel Application Platform (SNAP), version 8.0.0.

Table 2

Sentinel 3A images used, acquired from the Copernicus Open Access Hub service.

Number	Date (dd/mm/yyyy)	UTC Time (hhmm)	Cloudiness (%)	Sentinel 3A file name
1	March 08, 2019	10:25	8	S3A_SL_2_LST__20190308T102510_LN2_003.SEN3
2	March 12, 2019	10:21	3	S3A_SL_2_LST__20190312T102127_LN2_003.SEN3
3	March 27, 2019	10:32	12	S3A_SL_2_LST__20190327T103241_LN2_003.SEN3
4	April 10, 2019	09:54	4	S3A_SL_2_LST__20190410T095450_LN2_003.SEN3
5	April 29, 2019	10:02	5	S3A_SL_2_LST__20190429T100221_LN2_003.SEN3
6	May 02, 2019	10:24	8	S3A_SL_2_LST__20190502T102448_LN2_003.SEN3
7	May 08, 2019	11:09	12	S3A_SL_2_LST__20190508T110941_LN2_003.SEN3
8	May 21, 2019	10:06	3	S3A_SL_2_LST__20190521T100627_LN2_003.SEN3
9	June 03, 2019	09:54	4	S3A_SL_2_LST__20190603T095452_LN2_003.SEN3
10	June 20, 2019	10:28	7	S3A_SL_2_LST__20190620T102849_LN2_003.SEN3
11	March 08, 2020	10:08	6	S3A_SL_2_LST__20200308T102237_LN2_003.SEN3
12	March 12, 2020	10:43	11	S3A_SL_2_LST__20200312T101853_LN2_003.SEN3
13	March 27, 2020	10:13	6	S3A_SL_2_LST__20200327T103007_LN2_003.SEN3
14	April 10, 2020	10:20	12	S3A_SL_2_LST__20200410T100607_LN2_003.SEN3
15	April 19, 2020	10:24	0	S3A_SL_2_LST__20200429T101338_LN2_003.SEN3
16	May 02, 2020	10:09	1	S3A_SL_2_LST__20200502T103604_LN2_003.SEN3
17	May 08, 2020	10:26	13	S3A_SL_2_LST__20200508T105509_LN2_003.SEN3
18	May 21, 2020	11:05	5	S3A_SL_2_LST__20200521T101746_LN2_003.SEN3
19	June 03, 2020	10:35	3	S3A_SL_2_LST__20200603T101954_LN2_003.SEN3
20	June 20, 2020	10:21	1	S3A_SL_2_LST__20200620T104016_LN2_003.SEN3

Table 3

Sentinel 3B images used, acquired from the Copernicus Open Access Hub service.

Number	Date (dd/mm/yyyy)	UTC Time (hhmm)	Cloudiness (%)	Sentinel 3B file name
1	March 08, 2019	21:42	7	S3B_SL_2_LST__20190308T214205_LN2_003.SEN3
2	March 12, 2019	21:38	1	S3B_SL_2_LST__20190312T213821_LN2_003.SEN3
3	March 27, 2019	21:49	8	S3B_SL_2_LST__20190327T214936_LN2_003.SEN3
4	April 10, 2019	20:00	3	S3B_SL_2_LST__20190410T200045_LN2_003.SEN3
5	April 29, 2019	20:08	5	S3B_SL_2_LST__20190429T200817_LN2_003.SEN3
6	May 02, 2019	20:30	9	S3B_SL_2_LST__20190502T203043_LN2_003.SEN3
7	May 08, 2019	21:15	12	S3B_SL_2_LST__20190508T211537_LN2_003.SEN3
8	May 21, 2019	21:23	5	S3B_SL_2_LST__20190521T212332_LN2_003.SEN3
9	June 03, 2019	20:00	2	S3B_SL_2_LST__20190603T200048_LN2_003.SEN3
10	June 20, 2019	21:45	8	S3B_SL_2_LST__20190620T214544_LN2_003.SEN3
11	March 08, 2020	20:25	5	S3B_SL_2_LST__20200308T102237_LN2_003.SEN3
12	March 12, 2020	20:32	10	S3B_SL_2_LST__20200312T101853_LN2_003.SEN3
13	March 27, 2020	20:18	9	S3B_SL_2_LST__20200327T103007_LN2_003.SEN3
14	April 10, 2020	20:43	2	S3B_SL_2_LST__20200410T100607_LN2_003.SEN3
15	April 19, 2020	20:22	0	S3B_SL_2_LST__20200429T101338_LN2_003.SEN3
16	May 02, 2020	20:25	3	S3B_SL_2_LST__20200502T103604_LN2_003.SEN3
17	May 08, 2020	20:27	10	S3B_SL_2_LST__20200508T105509_LN2_003.SEN3
18	May 21, 2020	20:19	6	S3B_SL_2_LST__20200521T101746_LN2_003.SEN3
19	June 03, 2020	20:36	8	S3B_SL_2_LST__20200603T101954_LN2_003.SEN3
20	June 20, 2020	21:15	2	S3B_SL_2_LST__20200620T104016_LN2_003.SEN3

2.4. Environmental variables Pm_{10} , O_3 , Co , So_2 and No_2

The environmental variables taken into account in this research are the following: Pm_{10} , O_3 , Co , So_2 and No_2 . They are deemed key to assess the environmental quality of European cities according to Directive (2008)/50/CE of the European Parliament on air quality (EU, 2008). A number of studies regarding environmental quality rely on these variables (Lauri, 2020; Mandal and Pal, 2020; Mitra et al., 2020; Ali et al., 2021; Das et al., 2021). The values of the environmental variables for the dates selected, coinciding with the dates of the satellite images, were downloaded from the US-EPA Environmental Monitoring Network (<https://aqicn.org/map/spain/andalucia/>).

2.5. Land Surface Temperature estimation

Sentinel 3 products with processing level 1 require the use of split window algorithms, based on the concept of differential absorption (McMillin, 1975), for LST recovery. In view of the difference between the two TIRS bands in their wavelengths, the atmospheric effects produced on the signal can be corrected. They depend on the emissivity of the earth's surface, which can be obtained in multiple ways (Ruescas et al., 2016). The algorithm used internally by the official Sentinel 3A and 3B level 2 product is as follows (Remedios and Emsley, 2012):

$$LST = a_{f,i,pw} + b_{f,i}(T_{11} - T_{12})^{\frac{1}{\cos(\frac{\theta}{m})}} + (b_{f,i} + c_{f,i})T_{12} - 273.15, \quad (1)$$

where LST is the surface temperature in °C; a, b and c are coefficients dependent on the vegetation cover and the biome; and T_{11} and T_{12} are the brightness temperatures of bands 8 and 9 of Sentinel 3, respectively. θ is the zenith angle of view of the satellite, and m is a dependent variable of θ (Remedios and Emsley, 2012; Yang et al., 2020).

With the help of the open-source software Sentinel Application Platform (SNAP) version 7.0.0 and using level 2 products, the day and night LST of each investigated day was recovered for each city. These LST images were subsequently exported in Geotiff format to the open-source software QGIS, version 3.16.3, to determine the space-time variability of the SUHI for the eight cities.

2.6. Surface Urban Heat Island intensity

In the literature, SUHI intensity is defined as the difference in surface temperature between measurements within the urban area and in rural areas surrounding the city, taken at the same time (Oke, 1987). It can be determined with Equation (2):

$$SUHI = LST_{urban} - LST_{rural} \quad (2)$$

Having exported the LST images of Sentinel 3A and 3B to QGIS software, version 3.10.5, and with the help of the raster calculator command, the SUHI of the city was determined by means of Equation (2).

2.7. Satellite data validation

Values obtained through satellite images call for verification. In recent decades, for LST values, comparison with ambient temperatures is gaining importance as a validation method (Srivastava et al., 2009; Gallo et al., 2011; Liu and Zhang, 2011; Avdan and Jovanovska, 2016; Rongali et al., 2018; Mukherjee and Singh, 2020; Hidalgo and Arco, 2021). The recovered LST is compared with the ambient temperature obtained from meteorological stations or temperature probes located near the ground (1–2 m). In our research, the LSTs obtained through Sentinel 3 satellite images were validated against the environmental temperature values of AEMET stations during the hours of passage of the satellites. In order to minimize the impact of the rural environment on the subsequent calculation of the SUHI, we selected sites in rural areas, surrounded by farmland and having few impervious surfaces. This selection criterion has given statistically significant impacts in similar research efforts (Wang et al., 2017; Jiang et al., 2019).

2.8. Analytical strategy

Statistical analysis of the data collected in this study was performed with STATA software, version 15, using the Data Panel technique. This method is commonly used in the literature, and entails multivariate relationship models (Chen et al., 2011; Alcock et al., 2015; Fang and Tian, 2020) and a greater number of data, which increases the degrees of freedom in analysis while reducing the inconvenience of collinearity between variables (Smith and Hsiao, 1988). By accounting for individual effects, the final function obtained for the set of individual items is totally different from the one that would have been obtained using other statistical techniques (Labra, 2014). The method is recommended for dealing with time series involving multiple individual and quantitative variables, where explanatory variables in the relations between individuals might change (Seto and Kaufmann, 2003). Hence, this system of analysis was very well suited to the experimental data of our study.

Introducing this method of statistical analysis in our model involved two phases (Chen et al., 2011). Firstly, by means of the Hausman proof, the effects of analysis were determined to be either fixed or random. Then the model was assessed in view of the results obtained in Wooldridge and Wald Tests. There are three options for calculation: Method of Ordinary Squares (MOS), Generalized Least Squares (GLS) and the Method of Intragroup Estimators (MIE) (Labra, 2014).

The first of the three, while widely used for years, does not enable the effects of every individual to be analyzed over the course of time, which can give rise to biased estimations.

The second is considered to be a more efficient extension of the first. It is assumed that individual effects are not reflected in the explanatory variables of the model; instead, they contribute to the error term, following the expression:

$$Y_{it} = \beta X_{it} + (\alpha_i + \mu_{it}), \quad (3)$$

where α_i represents the individual effects, μ_{it} is the error of the model, and X would represent explanatory variables, i =individual and t =time.

The third method cited above assumes that individual effects are in line with the explanatory variables, so that the individual effect is separated after error, under the following calculation:

$$Y_{it} = \alpha_i + \beta X_{it} + \mu_{it}, \quad (4)$$

where, again, α_i are the individual effects, μ_{it} is the error of the model, and X are explanatory variables, i =individual and t =time.

3. Results

3.1. Statistical analysis

3.1.1. Satellite temperature validation

In order to validate the satellite data obtained, we proceeded to determine the coefficients of linear adjustment R^2 between the LST obtained with Sentinel 3A and 3B and the ambient temperatures acquired from AEMET. The results achieved are considered adequate, since they present values above 0.97 (Sentinel 3A: $R^2 = 0.991$; Sentinel 3B: $R^2 = 0.978$). The standard deviation (SD), mean bias error (MBE) and root mean squared error (RMSE) obtained for the Sentinel 3A data set were: SD = 8.68 °C; MBE = -0.129 °C and RMSE = 3.95 °C; while for Sentinel 3B, the values were: SD = 7.56 °C; MBE = -0.243 °C and RMSE = 3.05 °C. These values indicate a good agreement between the analyzed values and they are considered statistically significant above 97%.

3.1.2. LST and SUHI versus confinement situation

Statistical analysis using the Data Panel method was performed to determine if the situation of home confinement affects the LST and SUHI obtained in the investigated cities. First, it is necessary to determine whether the calculation procedure should be carried out using fixed or random effects. To this end, the Hausman test was implemented, obtaining that it was necessary to use the panel of robust random effects data for the data. To develop the Data Panel, the method of Generalized Least Squares (GLS) was used, by means of Equation (3). The results of the analysis of the day and night LST and SUHI data obtained from Sentinel 3A and 3B, respectively, are indicated in Tables 4 and 5.

The results of the statistical analysis of the LST and SUHI data related to the situation of home confinement obtained using Sentinel 3A indicate a statistically significant and negative relationship of 99% between the LST and SUHI variables and home confinement. With respect to Sentinel 3B, they give a statistically significant and negative relationship above 99% between the LST and SUHI variables and home confinement. The values obtained for R^2 , the F statistic of the data and the Prob > Chi² obtained for the LST using Sentinel 3A were: $R^2 = 0.63$; F = 18.15 and Prob > Chi² = 0.000. For Sentinel 3B, they were: $R^2 = 0.65$; F = 20.11 and Prob > Chi² = 0.000. The values obtained for the SUHI were: 3A: $R^2 = 0.42$; F = 6.23; Prob > Chi² = 0.018; for 3B they were: $R^2 = 0.39$; F = 3.17; Prob > Chi² = 0.048. These data are seen to indicate a good concordance between the dependent variable and the independent variable chosen by the method used, with a level of adjustment raised to 95% of significance, since Prob > Chi² < 0.005. Hence, there is good agreement between the SUHI and LST values and the confinement situation.

Table 4

LST results of confinement, Data Panel Sentinel 3A and 3B.

Satellite	Sentinel 3A			Sentinel 3B		
	β	p	sd	β	p	sd
Lockdown	-0.1254	0.005**	0.5638	-5.846	0.000***	1.3037
Constant	300.94	0.000***	1.5438	299.29	0.000***	2.1816

β : coefficient; sd: standard deviation; robust standard errors: * p <0.05.

** p <0.01 y *** p <0.001.

Table 5

SUHI results of confinement, Data Panel Sentinel 3A and 3B.

Satellite	Sentinel 3A			Sentinel 3B		
	β	p	sd	β	p	sd
Lockdown	-0.0321	0.006**	0.1180	-0.7087	0.001***	0.3978
Constant	-0.7766	0.027*	0.3441	2.0507	0.003**	0.6657

β : coefficient; sd: standard deviation; robust standard errors: * p <0.05.

** p <0.01 y *** p <0.001.

3.1.3. Contaminants versus confinement situation

Further statistical analysis was done using the Data Panel method to determine if the concentration of pollutants was affected by the situation of home confinement. As in the previous section, first, it was necessary to determine if the calculation procedure should be carried out using fixed or random effects. The Hausman test gave that the panel of robust random effects should be taken for the data. In applying the Data Panel, the method of Generalized Least Squares (GLS) was used through Equation (3). The results of data analysis regarding contaminants and the confinement situation are expressed in Table 6.

The results of the daytime pollution data related to the situation of home confinement indicate a statistically significant and negative relationship of 95% between the variable Pm_{10} and the situation of home confinement. For the nocturnal data, a statistically significant and negative relationship is observed above 99% with variable No_2 and 95% with variable Pm_{10} . The diurnal values obtained were as follows: $R^2 = 0.78$; $F = 1.25$ and $Prob > Chi^2 = 0.002$. The nocturnal values were: $R^2 = 0.36$; $F = 8.61$; $Prob > Chi^2 = 0.000$. These data show good concordance between the dependent variable and the independent variable chosen by the method used, with a level of adjustment raised to 95% significance, since $Prob > chi^2 < 0.005$. Again, there is good agreement between the UHI and LST values and the confinement situation.

3.1.4. LST and SUHI with pollutants by city typology

After determining with the previous steps that there is a statistically significant relationship between the LST and SUHI and the confinement situation and the pollutants, we went on with the statistical analysis to determine which pollutants condition the daytime and nighttime LST and SUHI both in inland cities and coastal cities. When determining whether the calculation procedure should be carried out using fixed or random effects, the Hausman test indicated that the panel of robust random effects should be applied. To develop the Data Panel, the method of Generalized Least Squares (GLS) was employed by means of Equation (3). The results of the pollutant analysis in terms of day and night LST are expressed in Tables 7 and 8.

Our findings regarding daytime data point to statistically significant relationships between LST and pollutants during the mornings without home confinement. However, during the period of home confinement, no statistically significant relationships appear between the dependent and independent variables. In inland cities and during the period without home confinement there is a statistically significant and positive relationship of 95% between the variable O_3 and the LST. In turn, a 95% negative relationship is seen between variable Co and LST, and 99% positive between variable No_2 and LST.

With the daytime data on the coastal cities, a statistically significant and negative relationship is observed above 99% for the variables Pm_{10} , negative, and of 99% for O_3 and positive for the variable Co; and positive 95% for the variable SO_2 . The diurnal values of the interior cities without confinement were: $R^2 = 0.80$; $F = 3.25$ and $Prob > Chi^2 = 0.002$, while the daytime values of the coastal cities were: $R^2 = 0.83$; $F = 8.12$; $Prob > Chi^2 = 0.000$. These data indicate a good concordance between the dependent variable and

Table 6
Contaminant versus confinement results, Data Panel.

Satellite	Sentinel 3A			Sentinel 3B		
	β	ρ	sd	β	ρ	sd
Pm_{10}	-0.0544	0.046*	0.0267	-0.0077	0.046*	0.0040
O_3	-0.0155	0.182	0.0115	-0.0010	0.468	0.0141
Co_2	0.0002	0.982	0.010	-0.0001	0.409	0.0001
SO_2	-0.0229	0.873	0.1434	0.0166	0.606	0.0320
No_2	-0.0065	0.770	0.2223	-0.0148	0.000***	0.0027
Constant	3.825	0.000***	1.0415	2.0890	0.000***	0.1594

β : coefficient; sd: standard deviation; robust standard errors: * $p < 0.05$.

** $p < 0.01$ y *** $p < 0.001$.

Table 7
Data panel results with Sentinel 3A by type of city and confinement situation.

	Diurnal without confinement						Diurnal with confinement					
	Inland Cities			Coastal cities			Inland Cities			Coastal cities		
	β	ρ	sd	β	ρ	sd	β	ρ	sd	β	ρ	sd
Pm_{10}	-0.0683	0.636	0.1443	-1.064	0.000***	0.0736	0.3932	0.194	0.3030	0.1186	0.689	0.2961
O_3	0.29932	0.041*	0.1466	-0.371	0.001**	0.1166	-0.032	0.879	0.2160	0.6086	0.552	0.1024
Co	-0.0223	0.023*	0.0097	0.009	0.009**	0.0035	0.009	0.580	0.1802	-0.013	0.313	0.1309
SO_2	0.9522	0.459	1.2871	5.557	0.033*	2.6101	0.9759	0.417	1.2030	1.3694	0.574	2.4349
No_2	0.2581	0.001**	0.0807	-0.025	0.638	0.0539	0.0782	0.748	0.2437	-0.021	0.850	0.1163
Constant	295.80	0.000	18.799	323.44	0.000	2.2221	285.41	0.000	7.1258	302.49	0.000	12.95

β : coefficient; sd: standard deviation; robust standard errors: * $p < 0.05$, ** $p < 0.01$ and *** $p < 0.001$.

Table 8

Data panel results with Sentinel 3B by type of city and confinement situation.

	Nocturnal without confinement						Nocturnal with confinement					
	Inland Cities			Coastal cities			Inland Cities			Coastal cities		
	β	ρ	sd	β	ρ	sd	β	ρ	sd	β	ρ	sd
Pm ₁₀	-0.2338	0.020*	0.1002	-0.0431	0.140	0.0291	-0.081	0.719	0.2266	-0.043	0.140	0.0291
O ₃	0.1012	0.022*	0.0443	-0.0134	0.588	0.0248	0.091	0.092	0.0544	-0.013	0.588	0.0248
Co	-0.0037	0.375	0.0041	0.0000	0.981	0.0017	-0.007	0.441	0.0102	0.000	0.981	0.0017
So ₂	0.7464	0.040*	0.3637	0.6174	0.480	0.8747	-2.771	0.139	1.8323	0.617	0.480	0.8747
No ₂	0.0512	0.464	0.0699	-0.0804	0.007**	0.2983	0.392	0.083	0.2261	-0.080	0.007**	0.0298
Constant	287.82	0.000***	6.0308	297.09	0.000	2.603	286.82	0.000***	1.9320	297.09	0.000***	2.6033

β: coefficient; sd: standard deviation; robust standard errors: *p<0.05, **p<0.01 and ***p<0.001.

the independent variable chosen by the method used, with a level of adjustment raised to 95% of significance, since Prob > Chi² < 0.005. Hence, there is good agreement between the pollutant values and the diurnal LST without confinement.

Statistical analysis of the nocturnal data (Table 8) report that during nights without home confinement, statistically significant relationships occur between the LST and the pollutants. In contrast, during the period of home confinement, statistically significant relationships were only found between the dependent and independent variables in coastal cities.

In inland cities and during the period without home confinement, there is a statistically significant and positive relationship of 95% between the variables O₃ and So₂. Yet the relationship is negative 95% between the variable Pm₁₀ and LST. Regarding nighttime data from coastal cities, a statistically significant and negative relationship of 99% is observed with variable No₂. The nocturnal values of the interior cities without confinement are as follows: R² = 0.83; F = 4.81 and Prob > Chi² = 0.001. The nighttime values of the coastal cities are: R² = 0.82; F = 5.12; Prob > Chi² = 0.000. Good concordance is observed between the dependent variable and the independent variable chosen by the method used, with a level of adjustment raised to 95% of significance, as Prob > Chi² < 0.005. This situation reflects good agreement between the pollutant values and the diurnal LST without confinement.

With respect to nighttime data from cities without confinement, a statistically significant and negative relationship can be reported at 99% with variable No₂ in coastal cities. The nocturnal values of the coastal cities with confinement are the following: R² = 0.84; F = 3.61 and Prob > Chi² = 0.003. Once again, these data indicate a good concordance between the dependent variable and the independent variable chosen, with a level of adjustment raised to 95% of significance, since Prob > Chi² < 0.005. This situation reflects good agreement between the pollutant values and the diurnal LST without confinement. No statistically significant relationships were discerned between the dependent variable SUHI and the independent polluting variables, either in inland cities or coastal cities, during confinement or non-confinement periods.

3.2. Environmental pollutants

The average daily air pollution values taken into account (So₂, Pm₁₀, No₂, Co) for the cities of study underwent significant reductions during the confinement period as compared to the average values from March to May of the year 2019 and the same period in 2020 when the confinement was not in force.

Contrariwise, O₃ values increased during the same period. Fig. 3 gives the mean daily reduction values of the investigated variables. The average reductions of the eight cities investigated amounted to: No₂ (-44.0%), Pm₁₀ (-38.3%), So₂ (-33.5%), and Co (-26.5%). The increase in variable O₃ was 5.9%. Yet the results demonstrate spatio-temporal variability in the reduction of pollutants, with differences between mornings and nights, and between coastal and inland cities. These results, corroborated by statistical analysis, confirm the importance of transport and industries on the high levels of environmental pollution in cities.

The mean diurnal reduction values of the investigated variables are reported in Fig. 4. As seen, the average daytime reductions of the eight cities surveyed are: No₂ (-36.9%), So₂ (-35.6%), Pm₁₀ (-34.5%), and Co (-28.7%). In contrast, variable O₃ showed an increase of 4.4%. Again, the pollutants of greatest and least reduction are No₂ and Co, respectively.

In Fig. 5 we find the mean nocturnal reduction values of the investigated variables: No₂ (-51.4%), Pm₁₀ (-43.0%), So₂ (-31.0%), and Co (-24.2%). The increase in variable O₃ was 6.9%. The pollutant presenting the greatest reduction at night is No₂, while the pollutant with the lowest nighttime reduction is Co.

The greatest average reductions of pollutants are found to occur during the night, with a value of 37.4% as opposed to the mornings when the reduction is 33.92%. It is noteworthy that the greatest reductions in So₂ and Co occur in the morning; and the greatest reductions in pollutants Pm₁₀ and No₂ occur at night. The greatest increase in variable O₃ also occurs at night. The nighttime decrease in pollutants could be related not only to the confinement situation, but also to the lower circulation of vehicles and a limited operation of industry when compared to daytime hours.

Figs. 6 and 7 show the reductions in both daytime and nighttime pollutants, but classified according to the geographic location of the cities: inland or coastal cities. They make manifest how the reduction of pollutants presents a high spatial variability between the two types of cities. The average daytime reductions (Fig. 6) of the inner cities were: No₂ (-47.5%), Pm₁₀ (-44.6%), Co (-28.6%), and So₂ (-16.9%). The increase in variable O₃ was 3.4%. The average daytime reductions of coastal cities were: So₂ (-45.3%), No₂ (-38.2%) Pm₁₀ (-22.7%), and Co (-14.2%); the increase in variable O₃ was 15.5%.

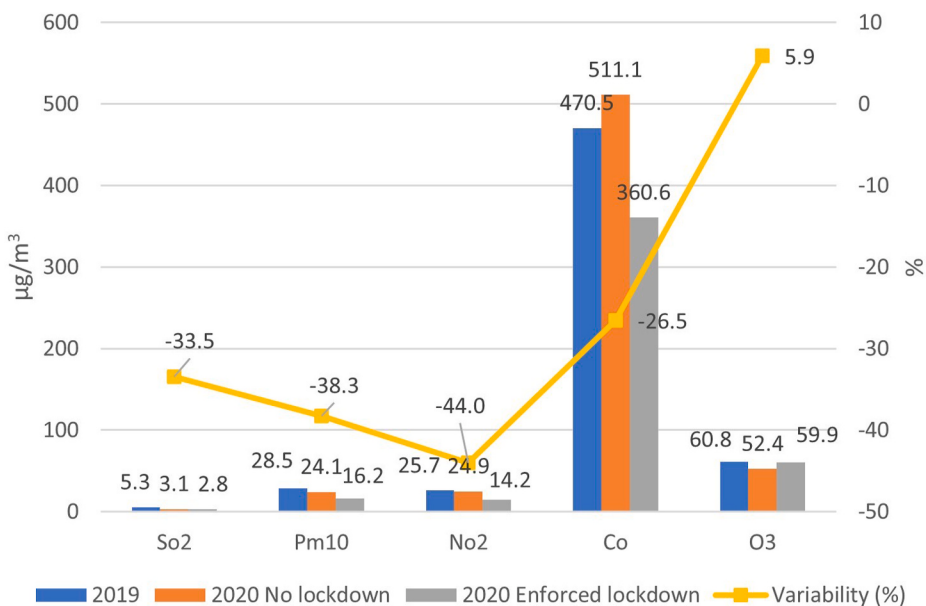


Fig. 3. Concentration of pollutants and average daily reduction in cities.

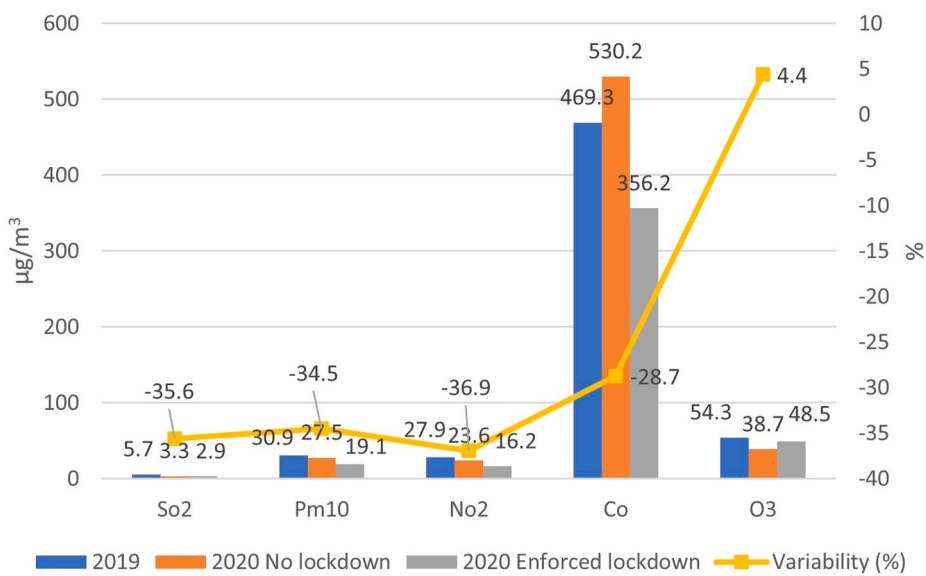


Fig. 4. Concentration of pollutants and average daytime reduction in cities.

The average nightly reductions (Fig. 7) of the inland cities were: NO₂ (-60.7%), Pm₁₀ (-49.6%), CO (-30.9%), and SO₂ (-12.7%). Variable O₃ increased by 3.3%. In turn, the average nightly reductions in coastal cities were: NO₂ (-57.1%), SO₂ (-43.4%), Pm₁₀ (-23.8%), and CO (-17.5%), whereas variable O₃ increased by 8.4%.

Therefore, the greatest daily reductions in pollutants Pm₁₀, NO₂ and CO occurred in inland cities, while the greatest reduction in SO₂ is seen for coastal cities, and O₃ grew the most in coastal cities. These data should be considered of great importance, since they indicate that the situation of home confinement caused by the COVID-19 pandemic produced a significant reduction in environmental pollutants, with the exception of O₃, both during the day and at night, in inland cities and coastal ones. The greater reduction in daytime pollutants in coastal cities could be related to sea breezes—they are known to flow from the sea towards the interior during the mornings, effectively cleaning the air to some extent.

3.3. Land Surface Temperatures versus ambient temperatures

The statistics of the LST obtained using the Sentinel 3A and 3B products and the environmental temperature recovered from the AEMET meteorological stations are shown in Fig. 8.

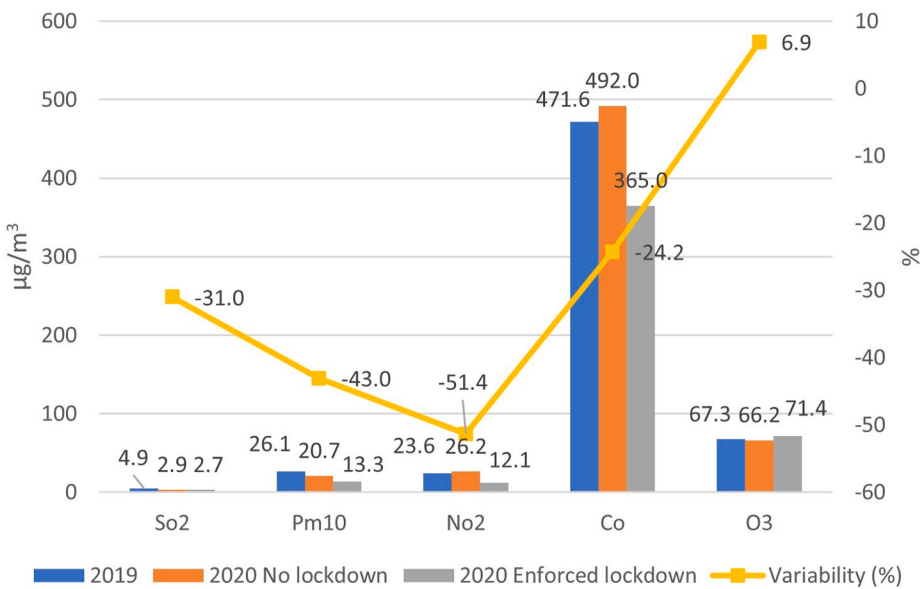


Fig. 5. Average concentration of pollutants and nighttime reduction in cities.

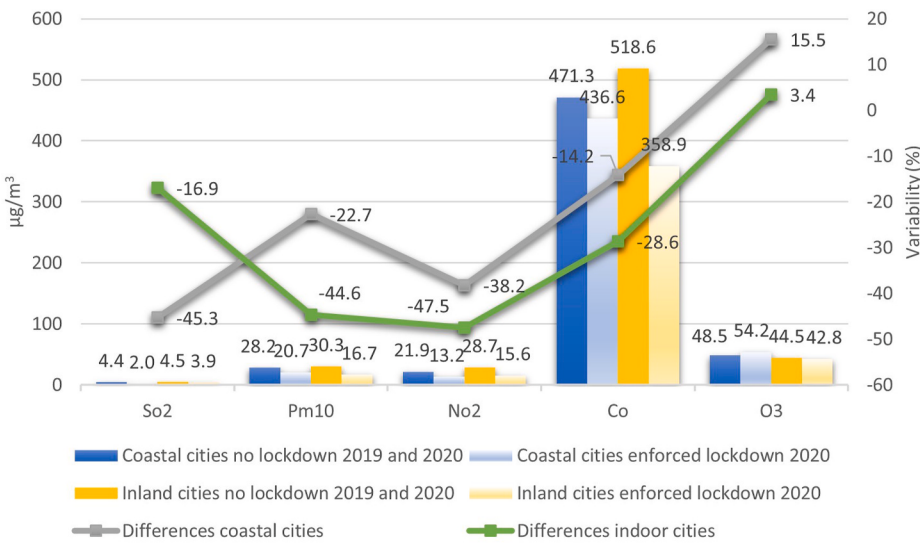


Fig. 6. Average concentration of pollutants and average daytime reduction by type of city.

In general terms, Sentinel 3A and 3B products present higher annual mean values for the eight cities investigated than those obtained in situ at meteorological stations. Specifically, in the morning, the highest mean values of LST were obtained with the official product Sentinel 3A (29.9 °C), as compared to the ambient temperature (26.8 °C). At night, the highest mean LST values were obtained with the official Sentinel 3B product (16.9 °C), the mean ambient temperature being lower (14.2 °C). The mean differences between the LST and the ambient temperature were 3.1 °C for Sentinel 3A and 2.7 °C for Sentinel 3B. However, Fig. 8 displays a positive asymmetry for the LST and ambient temperature data, concentrating the values in the third quartile. They present greater variability of the data in 25% of the low values, the difference being greater in the nocturnal values. These results are of great relevance; even though the temperatures are different, the two are clearly related, underlining the importance of future temperature involving LST and satellite images.

3.4. Land Surface Temperature versus confinement situation

Fig. 9 shows how the mean LST values obtained through Sentinel 3A images for the periods from March to May 2019 without home confinement are higher than the LST values obtained for the March to May 2020 home confinement period.

The diurnal LST values of the eight cities investigated are displayed in Fig. 10. During the confinement period, the LST values were significantly lower than during the non-confinement periods of 2019 and 2020. The mean LST decrease in the eight cities was

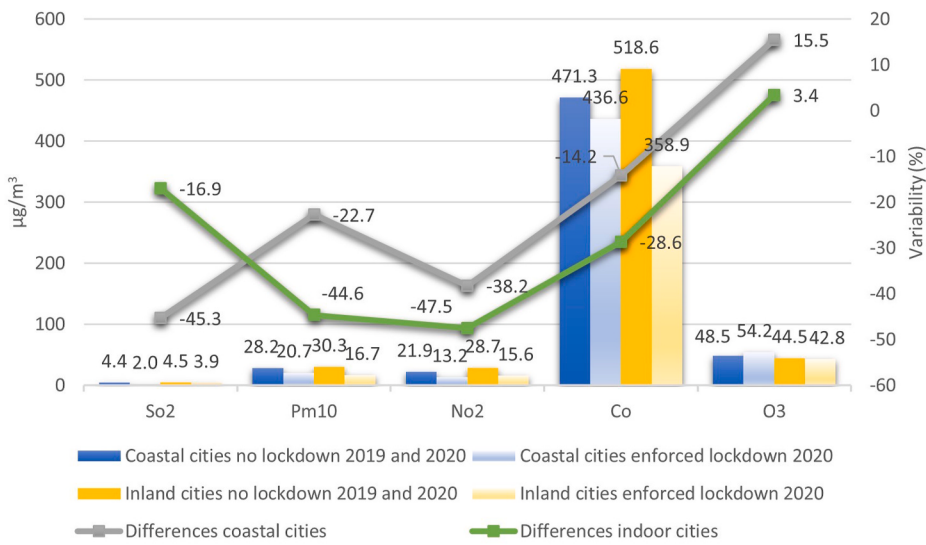


Fig. 7. Average concentration of pollutants and average nocturnal reduction by type of city.

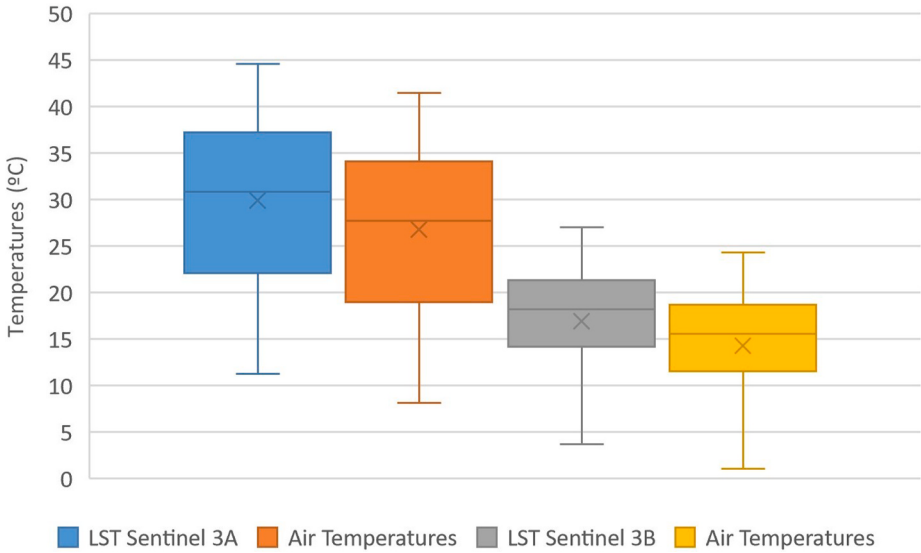


Fig. 8. LST Sentinel 3A and 3B statistics versus ambient temperatures.

$-4.0\text{ }^\circ\text{C}$, which represents an average reduction of -13.4% . The greatest daytime temperature reductions occurred in the cities of Granada ($-9.4\text{ }^\circ\text{C}$) and Almería ($-8.3\text{ }^\circ\text{C}$). To the contrary, the smallest reductions occurred in the cities of Jaén ($-0.5\text{ }^\circ\text{C}$) and Cádiz ($-1.9\text{ }^\circ\text{C}$). Such thermal differences might be motivated by the different climatic zones in which the corresponding cities are found: inland versus coastal areas. However, in this case a general reduction in LST values is seen for both types of cities. Some authors (Maithani et al., 2020; Mandal and Pal, 2020) have corroborated that a reduction in environmental pollution values leads to a reduction in the greenhouse effect, which allows long-wave radiation to escape into the atmosphere, leading to lower mean LST values.

Fig. 11 shows how the mean LST values obtained through Sentinel 3B images for the periods from March to May 2019 without home confinement are higher than the LST values obtained for the confinement periods.

Fig. 12 displays the diurnal LST values of the eight cities investigated. It is seen that during the confinement period the LST values were significantly lower than the values obtained during the non-confinement periods of the years 2019 and 2020. The average decrease in LST in the eight cities was $5.1\text{ }^\circ\text{C}$, which represents an average reduction of -25.1% . The greatest reductions in nighttime temperature are seen for the cities of Córdoba ($-8.6\text{ }^\circ\text{C}$) and Granada ($-7.8\text{ }^\circ\text{C}$). The smallest reductions correspond to Cádiz ($-2.3\text{ }^\circ\text{C}$) and Sevilla ($-3.0\text{ }^\circ\text{C}$).

As seen in Fig. 13, the reductions in LST generated by the situation of home confinement show strong spatio-temporal variability.

According to the data obtained with Sentinel 3A, the reduction in LST was greater in cities located on the coast, with a reduction of 15.2% ($-4.5\text{ }^\circ\text{C}$), than in inland cities, where the reduction was 11.6% ($-3.6\text{ }^\circ\text{C}$). Yet according to the data obtained by Sentinel 3B,

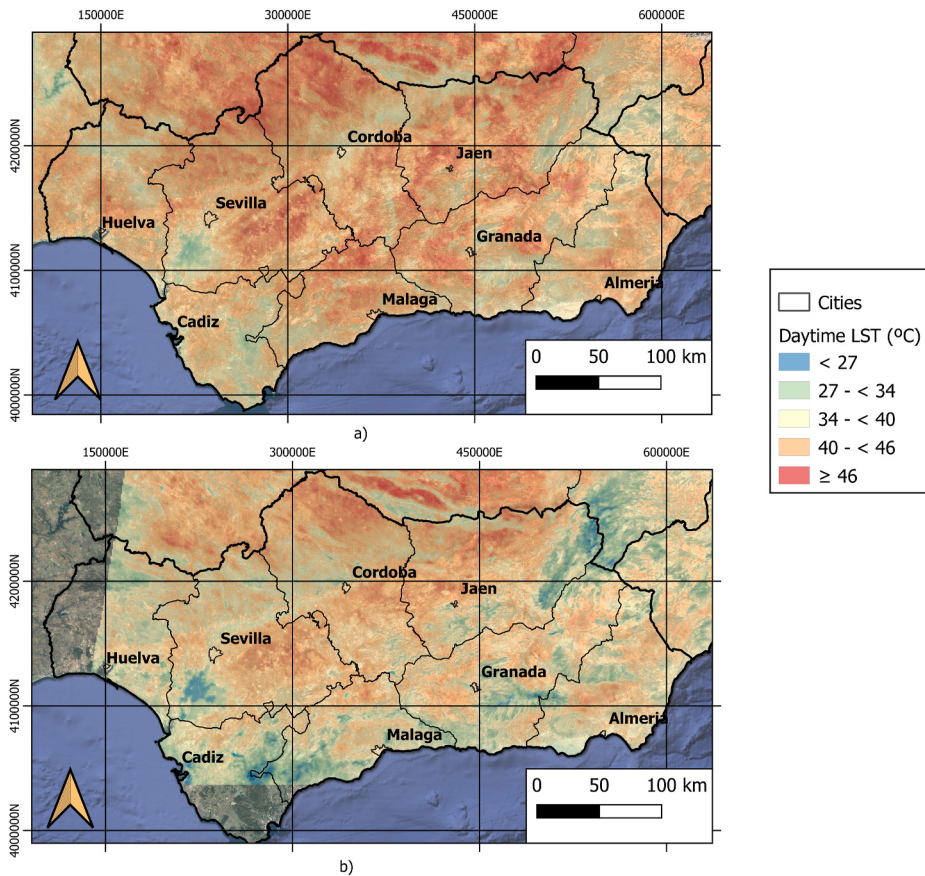


Fig. 9. LST Sentinel 3A, a) without confinement, b) with confinement.

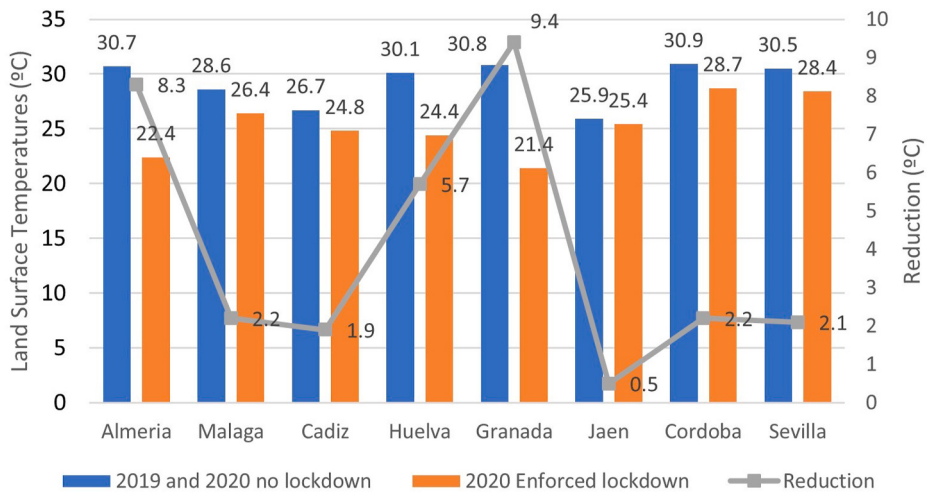


Fig. 10. Daytime mean LSTs by city and by study period.

the reduction was greater in inland cities, 30.7% (-5.9°C), as opposed to coastal cities, where the reduction in LST amounted to just 19.7% (-4.20°C). Therefore, we may affirm that the situation of home confinement caused by the COVID-19 pandemic led to a reduction in daytime and nighttime LST in the cities of study. Still, the LST reduction is greater during the night (5.1°C) than during the day (4.1°C). These results, confirmed by statistical analysis, highlight the importance of reducing environmental pollutants in order to reduce the LST of cities. Because a solid relationship between the LST and the concentrations of pollutants is verified, our results could orient future research efforts regarding possible LST mitigation measures. In short, LST mitigation solutions should be effective in reducing air pollution.

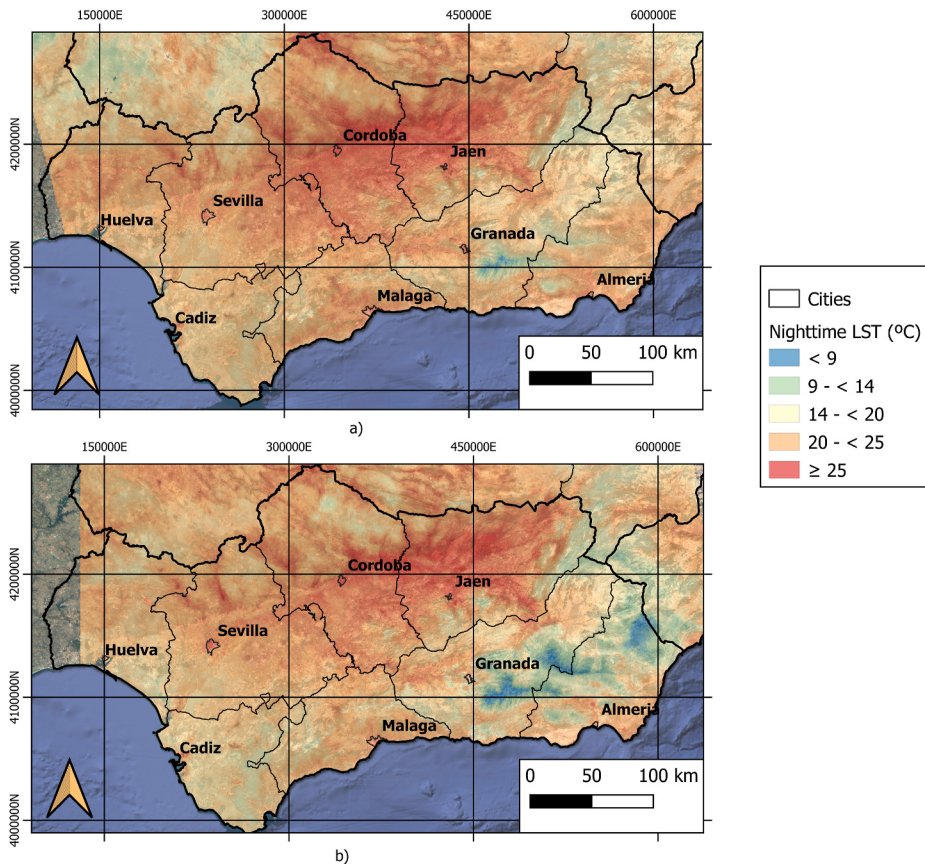


Fig. 11. LST Sentinel 3B, a) without confinement, b) with confinement.

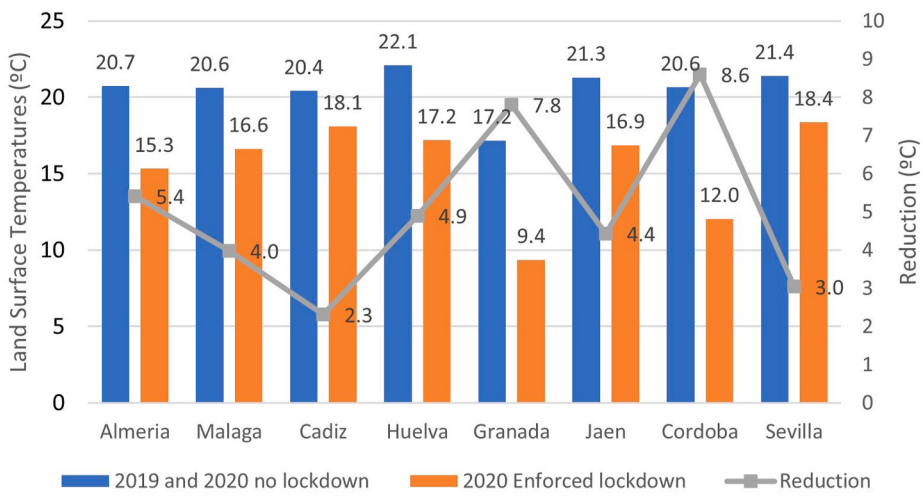


Fig. 12. Nightly average LST by city and by study period.

3.5. Surface Urban Heat Island intensity

The SUHI results reported here indicate significant daily mean reductions of this phenomenon: values between -0.33°C and -2.17°C , with a mean value of -1.02°C during the period of home confinement compared to the period without confinement of the years 2019 and 2020. Fig. 14 shows the diurnal SUHI values obtained with Sentinel 3A images for the periods from March to May of years 2019 and 2020 without home confinement, and the SUHI values obtained for the home confinement period of 2020. The average daytime intensity of the SUHI of the Andalusian cities during the 2019 and 2020 periods without confinement was -1.3°C , and during the confinement period it decreased to an average value of -0.4°C . These values give an average reduction of 0.9°C (69.23%).

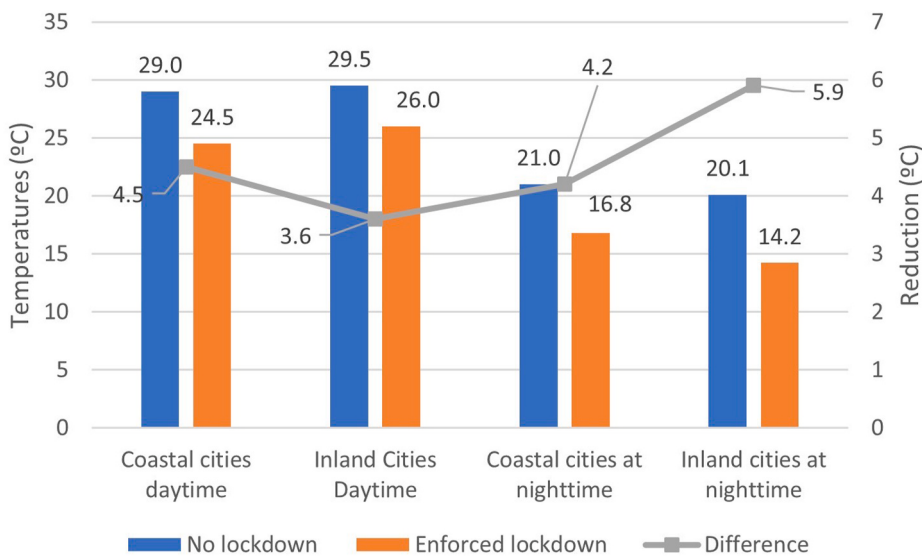


Fig. 13. Average reductions in LST according to type of city.

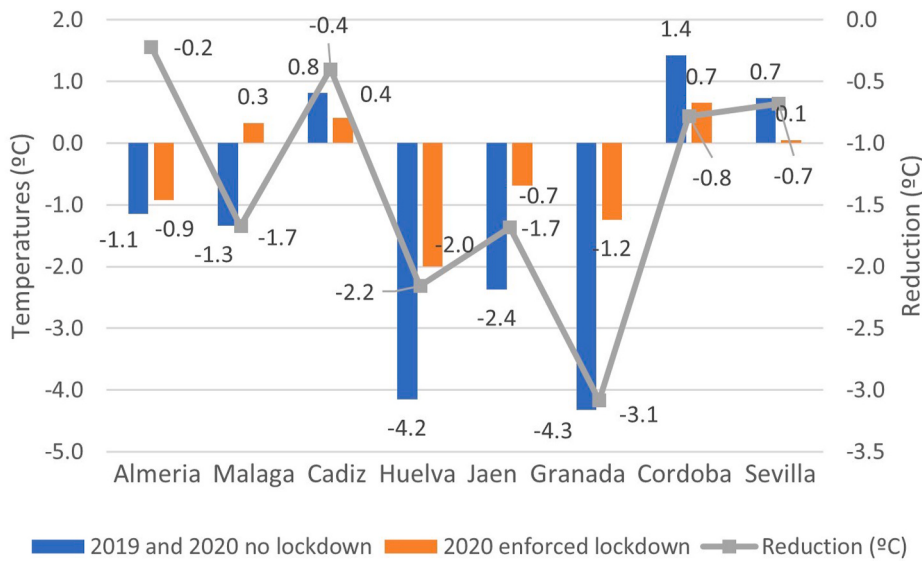


Fig. 14. Daytime mean SUHI by city and by study period.

The greatest reductions in SUHI intensity occurred in Granada (-3.1°C) and Jaen (-2.4°C). In turn, the smallest reductions were seen for Almeria (-0.2°C) and Cadiz (-0.4°C).

Obtaining SUHI with negative values implies that in the morning, the cities have lower temperatures than the surrounding rural areas. This situation has been previously studied by other authors, and is referred to as an urban cooling island (Saaroni et al., 2018; Wu et al., 2019; Yang et al., 2020a). During the early hours of the morning, solar radiation is higher in rural areas than in urban ones—owing to the shade of city buildings and trees, and the heterogeneous system of waterproof walls—and the thermal absorption and cooling rates of vegetated areas are high in comparison with the warming rates of areas having sparse vegetation or bare soils (Song et al., 2018; Yang et al., 2019; Fang and Tian, 2020; Yang et al., 2020a).

Fig. 15 offers the nocturnal SUHI values obtained using Sentinel 3B images for the periods from March to May of the years 2019 and 2020 without home confinement, along with the SUHI values obtained for the 2020 home confinement period. The mean nighttime intensity of the SUHI of the cities investigated, without confinement, was 1.3°C , and during the confinement period it dropped to 0.6°C . These values imply an average reduction of -0.7°C (53.84%). The greatest reductions in SUHI intensity occurred in the cities of Sevilla (-1.5°C) and Granada (-1.3°C). In contrast, the smallest reductions were seen for Malaga (-0.1°C) and Almeria and Cadiz (both -0.4°C). Obtaining SUHI with positive values means that during the night the cities analyzed have higher temperatures than the surrounding rural areas. This is because once the sun sets, rural areas tend to cool quickly, while urban areas retain heat. The use of waterproof building materials with high thermal absorption inside cities leads them, after the sun sets, to release the

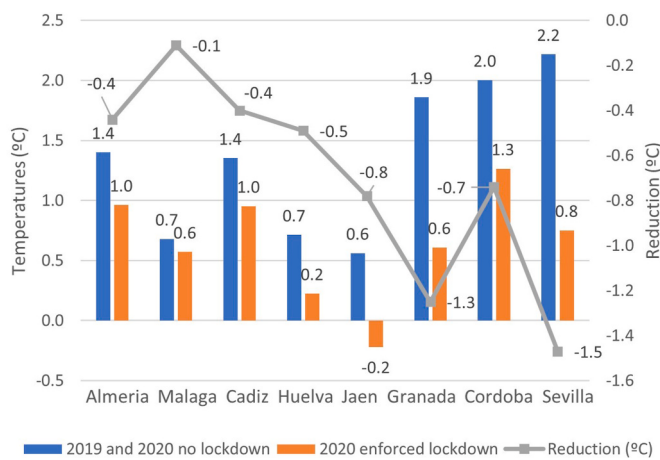


Fig. 15. SUHI nightly averages by city and by study period.

heat absorbed during the day. This urban heat island phenomenon has been previously studied by other authors (Saaroni et al., 2018; Wu et al., 2019; Yang et al., 2020a).

In Fig. 16 we see how the SUHI reductions in the investigated cities generated by the situation of home confinement present strong spatio-temporal variability. According to the data obtained through Sentinel 3A, the reduction in SUHI was lesser in cities located on the coast, with a reduction of -0.4°C (26.6%), than in inland cities, where the reduction was -0.2°C (40.0%). The data obtained by Sentinel 3B reflect a greater reduction in SUHI at night in coastal cities, -0.3°C (30.0%), in contrast to inland cities, where the reduction in SUHI was -0.1°C (14.3%).

Therefore, the situation of home confinement caused by the COVID-19 pandemic produced reductions in both daytime and nighttime UHI intensities, though somewhat greater during the day (-0.3°C) than at night (-0.2°C). These results are corroborated by the statistical analysis carried out. Hence, reducing environmental pollutants contributes to reducing UHI in cities. Future studies regarding possible mitigation measures of the UHI should take this finding into account; the solid relationship identified implies that UHI mitigation solutions could effectively reduce air pollution.

4. Discussion

The results reported in this research indicate significant reductions in the environmental pollutants analyzed, motivated by the period of home confinement decreed by the Government of Spain in view of the COVID-19 situation. The pollutants SO_2 , PM_{10} , NO_2 and CO presented average daily reductions of 33.5%, 38.3%, 44.0% and 26.5%, respectively. These data are in line with similar investigations in other cities or territories that underwent periods of home confinement (Mandal and Pal, 2020; Siddiqui et al., 2020;

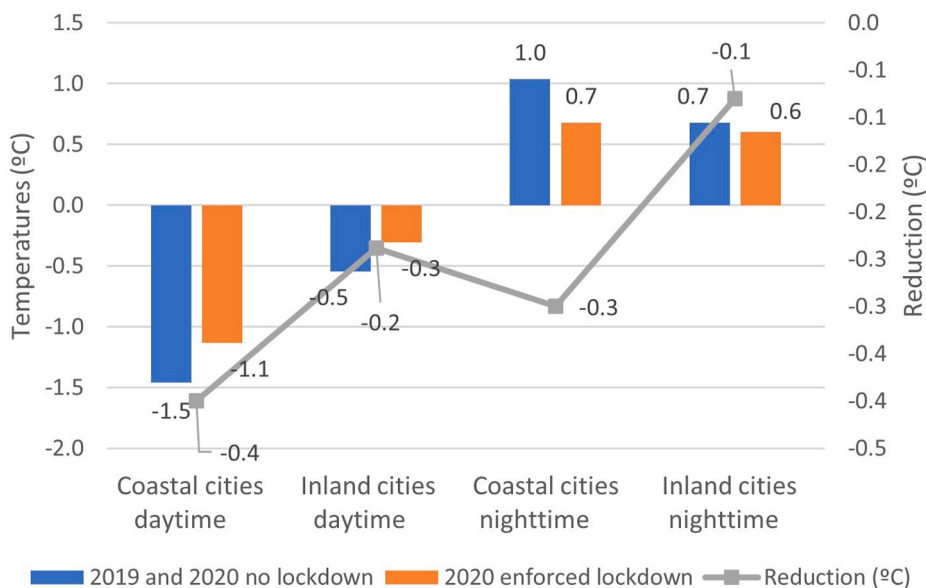


Fig. 16. Average SUHI reductions according to type of city.

Ali et al., 2021; Alqasemi et al., 2021; Das et al., 2021; Jiang et al., 2021), lending validity to the results obtained in our research. Therefore, it is corroborated that the confinement situation caused by COVID-19 had a positive impact by reducing the environmental pollutants discharged into the atmosphere. The variable O₃ presented an average daily increase of 5.9% during the period of home confinement. This finding may be attributed to the photochemical reaction caused by a high reduction of NO₂ emissions in the atmosphere (Li et al., 2016; Zou et al., 2019; Zhao et al., 2020).

Regarding the temporal variability of the reduction of pollutants, differences are observed between the daytime and nighttime values. The greatest reductions in pollutants occur at night; in the morning the average reduction is lower. The greatest daytime reductions are seen for pollutants SO₂ and Co, while the greatest nighttime reductions correspond to Pm₁₀ and NO₂. This circumstance could be influenced not only by the confinement situation but also by the lower pollution in the atmosphere at night compared to daytime hours. A number of studies report that daytime pollution in cities is greater than at night, owing to the circulation of public and private vehicles and to industrial activities that emit pollutants into the atmosphere (Bereitschaft and Debbage, 2013; Zhou et al., 2018; Wang et al., 2017). In this sense, it is corroborated that the greatest night-time reductions in pollutants are produced by pollutants from the combustion of vehicles and industries.

With respect to spatial variability, the greatest reductions in pollutants Pm₁₀, NO₂ and Co occur in inland cities, both during the day and at night, a circumstance caused by the wind direction in coastal areas. In the morning, sea breezes from the coastal areas flow landward, whereas at night the wind direction is towards the sea. Therefore, the night breeze can carry pollutants towards coastal areas, limiting their reductions with respect to inland areas (Morris and Simmonds, 2000; Jiang et al., 2019). The reduction of the pollutant SO₂, however, is greater in coastal cities than in inland cities. Taking into account that the highest concentrations of SO₂ come from maritime traffic, it is reasonable that the relative stoppage of transport and services due to the confinement produced a significant decrease of this pollutant in coastal cities (Zhou et al., 2018; Wang et al., 2017). As for the O₃ index, the highest daytime increase occurs in inland cities, considerably higher than the peak nighttime increase in coastal cities. Statistical analysis using the Data Panel technique reports stronger statistical relationships between the nocturnal LST and the nocturnal SUHI with the confinement situation in the cities of study. Higher statistical relationships are also seen between daytime and nighttime LST and contaminants in a non-confined situation—in contrast to the confinement situation, where no statistically significant relationships were found. These values agree with findings reported elsewhere, for coastal or inland areas that likewise had periods of home confinement (Mandal and Pal, 2020; Siddiqui et al., 2020; Ali et al., 2021; Alqasemi et al., 2021; Das et al., 2021; Jiang et al., 2021; Srivastava et al., 2021; Toro et al., 2021), supporting the results obtained in this investigation. Regarding the % reduction of the pollutant SO₂, our research indicates inverse results to the investigations carried out in nine cities in Pakistan (Ali et al., 2021) or in the country of South Korea (Ju et al., 2021), where no variations of this pollutant were reported during the period of home confinement.

The results presented on the level 2 products of Sentinel 3 for obtaining the LST and the SUHI give adequate yields, consistent with each other and similar to those of other studies (Li et al., 2011; Tan and Li, 2015; Sobrino et al., 2016; Prikaziuk and van der Tol, 2019; Yang et al., 2019; Chiang and Ivan, 2020; Hu et al., 2020; Ye et al., 2020). The precision of this method gives differences between the recovered LST and environmental temperatures that range between 0.2 and 7.8 °C (Gallo et al., 2011; Liu and Zhang, 2011; Avdan and Jovanovska, 2016; Rongali et al., 2018; Mukherjee and Singh, 2020). However, in other studies there are large differences in temperatures depending on whether the study is carried out in delimited urban areas or in large areas that include urban and rural zones. For example, authors Li et al. (2011), Avdan and Jovanovska (2016) and Mukherjee and Singh (2020) present temperature differences from 0.7 to 2.7 °C, but they involve delimited urban areas. To the contrary, authors Rongali et al. (2018) and Gallo et al. (2011) present temperature differences between 4 and 7 °C, applying to vast surfaces including both urban and rural areas.

The mean LSTs obtained in our research with Sentinel 3 products are higher than the ambient temperatures recorded at the meteorological stations. Thus, according to the data from Sentinel 3A, the mean daytime LST was 3.1 °C above the ambient temperature, while the difference was 2.7 °C for the case of Sentinel 3B. These values largely agree with the findings of Li et al. (2011), Avdan and Jovanovska (2016) and Mukherjee and Singh (2020), taking into account that our study area includes only urban areas. The coefficients of determination R², SD, MBE and RMSE denote a good agreement of the values and an adequate general performance. These data are in line with other reports from a number of cities or territories (Coppo et al., 2010; Ruescas et al., 2016; Sobrino et al., 2016; Prikaziuk and van der Tol, 2019; Chiang and Ivan, 2020; Yang et al., 2020b), lending validity to the results obtained in this research.

The LST results reported here indicate significant reductions during the period of home confinement as compared to the period without confinement in the years 2019 and 2020, results supported by the statistical analysis carried out. The LST reduction is clearly related to a reduction in pollution: the stoppage of activity led to a reduced greenhouse effect, which allowed long-wave radiation to escape into the atmosphere and decrease the LST values (Maithani et al., 2020; Mandal and Pal, 2020). More specifically, the mean daytime LST of the cities studied presented a lower average reduction, while the average night LST has presented a greater average reduction. Spatial variability results indicate that in the mornings, greater reduction in LST was detected in coastal cities as opposed to in inland cities. At night, greater reduction in LST took place in inland cities, however. These findings are in line with the results obtained in a study of the Dwarka River Basin (India), where LST reductions of between 3 and 5 °C were obtained (Mandal and Pal, 2020); in San Francisco Bay (USA), with an LST reduction between 5 and 8 °C (Potter and Alexander, 2021); or with the reductions detected in seven cities in Saudi Arabia (Alqasemi et al., 2021). Altogether, this circumstance indicates that the paralysis of tourism, industry and transport sectors caused by confinement significantly improves the temperature of the earth's surface. Yet our results are well above the values reported for the city of Tokyo (Fujibe, 2020), with values between -0.2 and -0.51 °C obtained through meteorological stations; those of Osaka (Nakajima et al., 2021), with a mean value of -0.13 °C obtained through numerical simulations using the Advanced Research WRF system; and Montreal (Canada) (Teufel et al., 2021), with a mean value of -1.0 °C obtained through high resolution simulations. Because the latter values were obtained by simulation, not from real measurements, they might be expected to differ from the actual results.

The SUHI results of our study and corresponding statistical analysis indicate significant reductions during the period of home confinement when compared to the period without confinement in years 2019 and 2020, giving an average value of -1.02°C (59.8%). In particular, the daytime UHI of the cities presented an average reduction greater than that of the nighttime UHI. Regarding spatial variability, it should be noted that during the mornings and nights the greatest reduction in UHI corresponds to coastal cities, being less in inland cities. Some authors ([Sabatino et al., 2020](#); [Schaefer et al., 2021](#)) underline the need to study environmental pollution, LST and UHI together, in such a way that any increase or reduction in environmental pollutants can be related with increases and decreases of the LST and UHI. These three elements are known to interact through the mixing, turbulence, and transfer processes of long-wave radiation. Therefore, mitigating any one of these three elements could serve to mitigate the other two. The values reported here are generally in line with the results obtained in seven cities in Saudi Arabia ([Alqasemi et al., 2021](#)), reporting reductions in night SUHI from 12.3% to 28.6%, with an average value of 19.2%; studies of nine cities in Pakistan ([Siddiqui et al., 2020](#)) where average SUHI reductions between -0.1°C (-8.7%) and -0.4°C (-19.5%) were obtained for major cities and megacities, respectively; or the high resolution simulations carried out in the city of Montreal (Canada) that gave reductions of -0.3 to -1.4°C ([Teufel et al., 2021](#)). In addition to supporting the results obtained in our research, such findings clearly indicate that the paralysis of tourism, industry and transport sectors as a consequence of confinement had a minimizing effect on the SUHI phenomenon.

5. Conclusions

The global situation generated by COVID-19 led to a widespread paralysis of key social and economic sectors due to periods of confinement decreed by different governments. This created a unique opportunity to assess the impact of human activity on environmental pollution, and to determine to what extent it may affect the urban climate, especially in terms of the phenomenon known as SUHI. Enhanced knowledge and characterization of extraordinary environmental situations is of great interest in order to establish mitigation and resilience measures in the framework of future urban development proposals.

The main objective of our work is to determine whether the situation of home confinement because of COVID-19 produced a reduction in environmental pollutants, and how it influenced the LST and SUHI of cities in Andalusia, southern Spain. To this end, satellite thermal images Sentinel 3A and 3B were used, which obtain LST images over cities with a time interval of 10–12 h. This made it possible to determine, first the LST, and then the SUHI, both during the daytime and at night, in periods of confinement (2020) and non-confinement (years 2019 and 2020). The use of Sentinel 3 images breaks with the tradition of working with only one satellite image per day. The methodology applied in this research, together with the morphological and geographic characteristics of the cities of Andalusia, an area highly prone to climate change, heighten the relevance of our results.

It can be concluded that the situation of home confinement gave rise to a significant reduction in environmental pollutants (Pm_{10} , SO_2 , NO_2 and Co) in the eight cities investigated. Meanwhile, pollutant O_3 increased its levels. There was spatial-temporal variability in the reduction of the pollutants analyzed: greater reductions at night than in the morning, and greater reductions in inland cities as opposed to coastal cities.

In association with the reduced pollution, a reduction in the LST and SUHI of cities because of the confinement situation was observed in comparison to the same dates in 2019 and 2020 without home confinement. The mean LST reduction was -4.6°C (-19.3%), being greater in the nocturnal measurements as opposed to the daytime ones. The greatest daytime reduction was seen for coastal cities; the greatest nighttime reduction occurred in inland cities. The mean reduction in SUHI was -1.0°C (-59.8%), the value being greater in daytime readings than in nighttime readings. The greatest reduction during both day and night occurred in coastal cities.

Sentinel 3 official products present higher average LSTs than those obtained through the AEMET meteorological stations. They show high precision and low sensitivity, working well on a global scale. They may therefore be considered adequate for estimating the LST and SUHI of the cities in the Andalusian region. Still, it is necessary to carry out further applied research to validate the precision of these products in cities located at other latitudes.

In the field of practice, our findings contribute to a comprehensive understanding of the environmental impact of human activity, and how halting it can reduce pollution and its effects on the LST and SUHI of cities. This information can help urban planners and public administrations in charge of managing future growth areas when they make decisions about the most appropriate mitigation measures to minimize the effects of LST and SUHI intensification. The distinction between coastal cities and inland cities is important. The results of studies like ours could be extrapolated to other cities in the Mediterranean Basin, given that the use of Sentinel 3 satellite images lies within the reach of the entire scientific community, and their use for determining LST and SUHI is straightforward.

Ethical statement

- 1) This material is the authors' own original work, which has not been previously published elsewhere.
- 2) The paper is not currently being considered for publication elsewhere.
- 3) The paper reflects the authors' own research and analysis in a truthful and complete manner.
- 4) The paper properly credits the meaningful contributions of co-authors and co-researchers.
- 5) The results are appropriately placed in the context of prior and existing research.
- 6) All sources used are properly disclosed (correct citation). Literally copying of text must be indicated as such by using quotation marks and giving proper reference.
- 7) All authors have been personally and actively involved in substantial work leading to the paper, and will take public responsibility for its content.

Declaration of competing interest

The authors declare that they have no known competing financial interests or personal relationships that could have appeared to influence the work reported in this paper.

References

- Alcock, I., White, M.P., Lovell, R., Higgins, S.L., Osborne, N.J., Husk, K., Wheeler, B.W., 2015. What accounts for "England's green and pleasant land"? A panel data analysis of mental health and land cover types in rural England. *Landsc. Urban Plann.* 142, 38–46. <https://doi.org/10.1016/j.landurbplan.2015.05.008>.
- Ali, G., Abbas, S., Qamer, F.M., Wong, M.S., Rasul, G., Irteza, S.M., Shahzad, N., 2021. Environmental impacts of shifts in energy, emissions, and urban heat island during the COVID-19 lockdown across Pakistan. *J. Clean. Prod.* 291, 125806. <https://doi.org/10.1016/j.jclepro.2021.125806>.
- Alqasemi, A.S., Hereher, M.E., Kaplan, G., Al-Quraishi, A.M.F., Saibi, H., 2021. Impact of COVID-19 lockdown upon the air quality and surface urban heat island intensity over the United Arab Emirates. *Sci. Total Environ.* 767, 144330. <https://doi.org/10.1016/j.scitotenv.2020.144330>.
- Andersson, D., Nässén, J., 2016. Should environmentalists be concerned about materialism? An analysis of attitudes, behaviours and greenhouse gas emissions. *J. Environ. Psychol.* 48, 1–11. <https://doi.org/10.1016/j.jenvp.2016.08.002>.
- Arbuthnott, K.G., Hajat, S., 2017. The health effects of hotter summers and heat waves in the population of the United Kingdom: a review of the evidence. *Environ. Health Global Acc. Sci. Source* 16 (Suppl. 1), 1–13. <https://doi.org/10.1186/s12940-017-0322-5>.
- Arnfield, A.J., 2003. Two decades of urban climate research: a review of turbulence, exchanges of energy and water, and the urban heat island. *Int. J. Climatol.* 23 (1), 1–26. <https://doi.org/10.1002/joc.859>.
- Avdan, U., Jovanovska, G., 2016. Algorithm for automated mapping of land surface temperature using LANDSAT 8 satellite data. *J. Sensors*, 2016. <https://doi.org/10.1155/2016/1480307>.
- Bashir, M.F., Ma, B., Bilal, Komal, B., Bashir, M.A., Tan, D., Bashir, M., 2020. Correlation between climate indicators and COVID-19 pandemic in New York, USA. *Sci. Total Environ.* 728, 138835. <https://doi.org/10.1016/j.scitotenv.2020.138835>.
- Bereitschaft, B., Debbage, K., 2013. Urban form, air pollution, and CO₂ emissions in large U.S. Metropolitan areas. *Prof. Geogr.* 65 (4), 612–635. <https://doi.org/10.1080/00330124.2013.799991>.
- Čeplová, N., Kalusová, V., Lososová, Z., 2017. Effects of settlement size, urban heat island and habitat type on urban plant biodiversity. *Landsc. Urban Plann.* 159, 15–22. <https://doi.org/10.1016/j.landurbplan.2016.11.004>.
- Chen, Y., Li, X., Zheng, Y., Guan, Y., Liu, X., 2011. Estimating the relationship between urban forms and energy consumption: a case study in the Pearl River Delta, 2005–2008. *Landsc. Urban Plann.* 102 (1), 33–42. <https://doi.org/10.1016/j.landurbplan.2011.03.007>.
- Chiang, S., Ivan, N., 2020. Mapping and tracking forest burnt areas in the indio maiz biological reserve using sentinel-3 SLSTR and VIIRS-DNB imagery. *Sensors* 19 (2019).
- Coleman, R.W., Stavros, N., Hulley, G., Parazoo, N., 2020. Comparison of thermal infrared-derived maps of irrigated and non-irrigated vegetation in urban and non-urban areas of southern California. *Rem. Sens.* 12 (24), 1–19. <https://doi.org/10.3390/rs12244102>.
- Coppo, P., Ricciarelli, B., Brandani, F., Delderfield, J., Ferlet, M., Mutlow, C., Munro, G., Nightingale, T., Smith, D., Bianchi, S., Nicol, P., Kirschstein, S., Hennig, T., Engel, W., Frerick, J., Nieke, J., 2010. SLSTR: a high accuracy dual scan temperature radiometer for sea and land surface monitoring from space. *J. Mod. Opt.* 57 (18), 1815–1830. <https://doi.org/10.1080/09500340.2010.503010>.
- Cramer, W., Guiot, J., Fader, M., Garraouji, B., Gattuso, J.P., Iglesias, A., Lange, M.A., Lionello, P., Llasat, M.C., Paz, S., Peñuelas, J., Snoussi, M., Toreti, A., Tsimplis, M.N., Xoplaki, E., 2018. Climate change and interconnected risks to sustainable development in the Mediterranean. *Nat. Clim. Change* 8 (11), 972–980. <https://doi.org/10.1038/s41558-018-0299-2>.
- Das, N., Sutradhar, S., Ghosh, R., Mondal, P., 2021. Asymmetric nexus between air quality index and nationwide lockdown for COVID-19 pandemic in a part of Kolkata metropolitan, India. *Urban Clim.* 36 (January), 100789. <https://doi.org/10.1016/j.uclim.2021.100789>.
- de Castro, M., Gallardo, C., Jylha, K., Tuomenvirta, H., 2007. The use of a climate-type classification for assessing climate change effects in Europe from an ensemble of nine regional climate models. *Climatic Change* 81 (S1), 329–341. <https://doi.org/10.1007/s10584-006-9224-1>.
- Diallo, J., Lacaze, B., Comby, J., 2015. Land surface temperature in the urban area of Lyon metropolis: a comparative study of remote sensing data and MesoNH model simulation. *2015 Joint Urban Remote Sensing Event. JURSE* 2–5, 2015. <https://doi.org/10.1109/JURSE.2015.7120528>.
- Du, J., Xiang, X., Zhao, B., Zhou, H., 2020. Impact of urban expansion on land surface temperature in Fuzhou, China using Landsat imagery. *Sustain. Cities Soc.* 61 (June), 102346. <https://doi.org/10.1016/j.scs.2020.102346>.
- Dwivedi, A., Mohan, B.K., 2018. Impact of green roof on micro climate to reduce Urban Heat Island. *Rem. Sens. Appl.: Soc. Environ.* 10, 56–69. <https://doi.org/10.1016/j.rsase.2018.01.003>.
- European Union (EU), 2008. Council Directive 2008/50, of May 21, 2008 on environmental air quality and a cleaner atmosphere in Europe. *Off. J. Euro. Union* 1–44, L152. 06/11/2002.
- Fang, L., Tian, C., 2020. Construction land quotas as a tool for managing urban expansion. *Landsc. Urban Plann.* 195 (May 2019), 103727. <https://doi.org/10.1016/j.landurbplan.2019.103727>.
- Feizizadeh, B., Blaschke, T., 2013. Examining Urban Heat Island relations to land use and air pollution: multiple endmember spectral mixture analysis for thermal remote sensing. *IEEE J. Selected Topics Appl. Earth Observ. Rem. Sens.* 6 (3), 1749–1756. <https://doi.org/10.1109/JSTARS.2013.2263425>.
- Fujibe, F., 2020. Temperature anomaly in the Tokyo metropolitan area during the COVID-19 (coronavirus) self-restraint period. *Sci. Online Lett. Atmos.* 16, 175–179. <https://doi.org/10.2151/SOLA.2020-030>.
- Gallo, K., Hale, R., Tarpley, D., Yu, Y., 2011. Evaluation of the relationship between air and land surface temperature under clear- and cloudy-sky conditions. *J. Appl. Meteorol. Climatol.* 50 (3), 767–775. <https://doi.org/10.1175/2010JAMC2460.1>.
- Ghosh, S., Das, A., Hembram, T.K., Saha, S., Pradhan, B., Alamri, A.M., 2020. Impact of COVID-19 induced lockdown on environmental quality in four Indian megacities Using Landsat 8 OLI and TIRS-derived data and Mamdani fuzzy logic modelling approach. *Sustainability* 12 (13), 1–24. <https://doi.org/10.3390/su12135464>.
- Guo, A., Yang, J., Xiao, X., Xia, C., Jin, C., Li, X., 2020. Influences of urban spatial form on urban heat island effects at the community level in China. *Sustain. Cities Soc.* 53, 101972. <https://doi.org/10.1016/j.scs.2019.101972>.
- He, G., Pan, Y., Tanaka, T., 2020. COVID-19, city lockdowns, and air pollution: evidence from China. *MedRxiv*. <https://doi.org/10.1101/2020.03.29.20046649>.
- Hidalgo, D., Arco, J., 2021. Modeling of the Urban Heat Island on local climatic zones of a city using Sentinel 3 images: urban determining factors. *Urban Clim.* 37, 100848. <https://doi.org/10.1016/j.uclim.2021.100840>.
- Hu, Y., Dai, Z., Guldmann, J.M., 2020. Modeling the impact of 2D/3D urban indicators on the urban heat island over different seasons: a boosted regression tree approach. *J. Environ. Manag.* 266 (11), 110424. <https://doi.org/10.1016/j.jenvman.2020.110424>.
- Hua, L., Zhang, X., Nie, Q., Sun, F., Tang, L., 2020. The impacts of the expansion of urban impervious surfaces on urban heat islands in a coastal city in China. *Sustainability* 12 (2). <https://doi.org/10.3390/su12020475>.
- Huang, X., Ding, A., Gao, J., Zheng, B., Zhou, D., Qi, X., Tang, R., Wang, J., Ren, C., Nie, W., Chi, X., Xu, Z., Chen, L., Li, Y., Che, F., Pang, N., Wang, H., Tong, D., Qin, W., He, K., 2021. Enhanced secondary pollution offset reduction of primary emissions during COVID-19 lockdown in China. *Natl. Sci. Rev.* 8 (2). <https://doi.org/10.1093/nsr/nwaa137>.
- Jiang, P., Fu, X., Fan, Y., Klemeš, J., Chen, P., Ma, S., Zhang, W., 2021. Spatial-temporal potential exposure risk analytics and urban sustainability impacts related to COVID-19 mitigation: a perspective from car mobility behaviour. *J. Clean. Prod.* 279. <https://doi.org/10.1016/j.jclepro.2020.123673>.
- Jiang, S., Lee, X., Wang, J., Wang, K., 2019. Amplified urban heat islands during heat wave periods. *J. Geophys. Res.: Atmos.* 124 (14), 7797–7812. <https://doi.org/10.1029/2018JD030230>.
- Ju, M.J., Oh, J., Choi, Y.H., 2021. Changes in air pollution levels after COVID-19 outbreak in Korea. *Sci. Total Environ.* 750, 141521. <https://doi.org/10.1016/j.scitotenv.2021.141521>.

- j.scitotenv.2020.141521.
- Labra, R., 2014. Zero Panel Data Guide. (Cátedra UA). file:///U:/Maguileria/Documentos Personales MAGUILERA/Master M3F/Trabajo Fin M3F/Revisión para paper/Referencias/Stata/16_Guía CERO para datos de panel_Un enfoque práctico.pdf.
- Lauri, M., 2020. Analysis: Coronavirus temporarily reduced China's CO2 emissions by a quarter. Carbon Brief. 2020. <https://www.carbonbrief.org/analysis-coronavirus-has-temporarily-reduced-chinas-co2-emissions-by-a-quarter>. (Accessed 21 November 2021).
- Lauri, M., 2020. Analysis: corona virus has temporarily reduced Chins's CO2 emissions by534 a quarter. <https://www.carbonbrief.org/analysis-coronavirus-has-temporarily-reduced-chinas-co2-emissions-by-a-quarter>.
- Lemus-Canovas, M., Martin-Vide, J., Moreno-Garcia, M.C., Lopez-Bustins, J.A., 2020. Estimating Barcelona's metropolitan daytime hot and cold poles using Landsat-8 Land Surface Temperature. *Sci. Total Environ.* 699, 134307. <https://doi.org/10.1016/j.scitotenv.2019.134307>.
- Li, J., Song, C., Cao, L., Zhu, F., Meng, X., Wu, J., 2011. Impacts of landscape structure on surface urban heat islands: a case study of Shanghai, China. *Rem. Sens. Environ.* 115 (12), 3249–3263. <https://doi.org/10.1016/j.rse.2011.07.008>.
- Li, M., Song, Y., Mao, Z., Liu, M., Huang, X., 2016. Impacts of thermal circulations induced by urbanization on ozone formation in the Pearl River Delta region, China. *Atmos. Environ.* 127 (2), 382–392. <https://doi.org/10.1016/j.atmosenv.2015.10.075>.
- Liu, L., Zhang, Y., 2011. Urban heat island analysis using the landsat TM data and ASTER Data: a case study in Hong Kong. *Rem. Sens.* 3 (7), 1535–1552. <https://doi.org/10.3390/rs3071535>.
- Logan, T.M., Zaitchik, B., Guikema, S., Nisbet, A., 2020. Night and day: the influence and relative importance of urban characteristics on remotely sensed land surface temperature. *Rem. Sens. Environ.* 247 (June 2019), 111861. <https://doi.org/10.1016/j.rse.2020.111861>.
- Macintyre, H.L., Heaviside, C., Taylor, J., Picetti, R., Symonds, P., Cai, X.M., Vardoulakis, S., 2018. Assessing urban population vulnerability and environmental risks across an urban area during heatwaves – implications for health protection. *Sci. Total Environ.* 610–611, 678–690. <https://doi.org/10.1016/j.scitotenv.2017.08.062>.
- Maithani, S., Nautiyal, G., Sharma, A., 2020. Investigating the effect of lockdown during COVID-19 on land surface temperature: study of Dehradun city, India. *J. Indian Soc. Rem. Sens.* 48 (9), 1297–1311. <https://doi.org/10.1007/s12524-020-01157-w>.
- Mandal, I., Pal, S., 2020. COVID-19 pandemic persuaded lockdown effects on environment over stone quarrying and crushing areas. *Sci. Total Environ.* 732 (May 2020), 139281. <https://doi.org/10.1016/j.scitotenv.2020.139281>.
- McMillin, L.M., 1975. Estimation of sea surface temperatures from two infrared window measurements with different absorption. *J. Geophys. Res.* 80 (36), 5113–5117. <https://doi.org/10.1029/jc080i036p05113>.
- Mitra, A., Ray Chaudhuri, T., Mitra, A., Pramanick, P., Zaman, S., 2020. Impact of COVID-19 related shutdown on atmospheric carbon dioxide level in the city of Kolkata. *Parana J. Sci. Educ.* 6 (3), 84–92. <https://sites.google.com/site/pjsciencea>.
- Morris, C., Simmonds, S., 2000. Associations between varying magnitudes of the urban heat island and the synoptic climatology in Melbourne, Australia. *Int. J. Climatol.* 20, 15. [https://doi.org/10.1002/1097-0088\(200012\)20:15<1931::AID-JOC578>3.0.CO;2-D](https://doi.org/10.1002/1097-0088(200012)20:15<1931::AID-JOC578>3.0.CO;2-D).
- Mukherjee, F., Singh, D., 2020. Assessing land use–land cover change and its impact on land surface temperature using LANDSAT data: a comparison of two urban areas in India. *Earth Syst. Environ.* 4 (2), 385–407. <https://doi.org/10.1007/s41748-020-00155-9>.
- Nakajima, K., Takane, Y., Kikegawa, Y., Furuta, Y., Takamatsu, H., 2021. Human behaviour change and its impact on urban climate: restrictions with the G20 Osaka Summit and COVID-19 outbreak. *Urban Clim.* 35 (October 2020), 100728. <https://doi.org/10.1016/j.uclim.2020.100728>.
- Oke, T.R., 1987. *Boundary Layer Climates*. Routledge.
- Pani, S.K., Lin, N.H., RavindraBabu, S., 2020. Association of COVID-19 pandemic with meteorological parameters over Singapore. *Sci. Total Environ.* 740, 140112. <https://doi.org/10.1016/j.scitotenv.2020.140112>.
- Potter, C., Alexander, O., 2021. Impacts of the San Francisco Bay Area shelter-in-place during the COVID-19 pandemic on urban heat fluxes. *Urban Clim.* 37 (November 2020), 100828. <https://doi.org/10.1016/j.uclim.2021.100828>.
- Prikaziuk, E., van der Tol, C., 2019. Global sensitivity analysis of the SCOPE model in Sentinel-3 Bands: thermal domain focus. *Rem. Sens.* 11 (20). <https://doi.org/10.3390/rs11202424>.
- Ray, D., Salvatore, M., Bhattacharyya, R., Wang, L., Du, J., Mohammed, S., Purkayastha, S., Halder, A., Rix, A., Barker, D., Kleinsasser, M., Zhou, Y., Bose, D., Song, P., Banerjee, M., 2020. Predictions, role of interventions and effects of a historic national lockdown in India's response to the the COVID-19 pandemic: data science call to arms. *Harvard Data Sci. Rev.* 1. <https://doi.org/10.1162/99608f92.60e08ed5>.
- Remedios, J., Emsley, S., 2012. *Sentinel-3 Optical Products and Algorithm Definition Land Surface Temperature*, vol. 24.
- Rongali, G., Keshari, A.K., Gosain, A.K., Khosa, R., 2018. A mono-window algorithm for land surface temperature estimation from landsat 8 thermal infrared sensor data: a case study of the Beas river basin, India. *Pertanika J. Sci. Technol.* 26 (2), 829–840.
- Roy, S., Pandit, S., Eva, E.A., Bagmar, M.S.H., Papia, M., Banik, L., Dube, T., Rahman, F., Razi, M.A., 2020. Examining the nexus between land surface temperature and urban growth in Chattogram Metropolitan Area of Bangladesh using long term Landsat series data. *Urban Clim.* 32 (January), 100593. <https://doi.org/10.1016/j.uclim.2020.100593>.
- Ruescas, A.B., Danne, O., Fomferra, N., Brockmann, C., 2016. The land surface temperature synergistic processor in beam: a prototype towards sentinel-3. *Data* 1 (3), 1–14. <https://doi.org/10.3390/data1030018>.
- Saaroni, H., Amorim, J.H., Hiemstra, J.A., Pearlmutter, D., 2018. Urban Green Infrastructure as a tool for urban heat mitigation: survey of research methodologies and findings across different climatic regions. *Urban Clim.* 24 (October 2017), 94–110. <https://doi.org/10.1016/j.uclim.2018.02.001>.
- Sabatino, S., Barbano, F., Brattich, E., Pulvirenti, B., 2020. The multiple-scale nature of urban heat island and its footprint on air quality in real urban environment. *Atmosphere* 11, 1186. <https://doi.org/10.3390/atmos11111186>.
- Santamouris, M., 2020. Recent progress on urban overheating and heat island research. Integrated assessment of the energy, environmental, vulnerability and health impact. Synergies with the global climate change. *Energy Build.* 207. <https://doi.org/10.1016/j.enbuild.2019.109482>.
- Sarrat, C., Lemonsu, A., Masson, V., Guedalia, D., 2006. Impact of urban heat island on regional atmospheric pollution. *Atmos. Environ.* 40 (10), 1743–1758. <https://doi.org/10.1016/j.atmosenv.2005.11.037>.
- Schwarz, N., Lautenbach, S., Seppelt, R., 2011. Exploring indicators for quantifying surface urban heat islands of European cities with MODIS land surface temperatures. *Rem. Sens. Environ.* 115 (12), 3175–3186. <https://doi.org/10.1016/j.rse.2011.07.003>.
- Schaefer, M., Ebrahimi, H., Kockler, H., Xuan, N., 2021. Assessing local heat stress and air quality with the use of remote sensing and pedestrian perception in urban microclimate simulations. *Sci. Total Environ.* 794, 148709. <https://doi.org/10.1016/j.scitotenv.2021.148709>.
- Seto, K.C., Kaufmann, R.K., 2003. Modeling the drivers of urban land use change in the Pearl River Delta, China: integrating remote sensing with socioeconomic data. *Land Econ.* 79 (1), 106–121. <https://doi.org/10.2307/3147108>.
- Shafizadeh-Moghadam, H., Weng, Q., Liu, H., Valavi, R., 2020. Modeling the spatial variation of urban land surface temperature in relation to environmental and anthropogenic factors: a case study of Tehran, Iran. *GIScience Remote Sens.* 57 (4), 483–496. <https://doi.org/10.1080/15481603.2020.1736857>.
- Siddiqui, A., Halder, S., Chauhan, P., Kumar, P., 2020. COVID-19 pandemic and city-level nitrogen dioxide (NO₂) reduction for urban centres of India. *J. Indian Soc. Rem. Sens.* 48 (7), 999–1006. <https://doi.org/10.1007/s12524-020-01130-7>.
- Smith, R.J., Hsiao, C., 1988. Analysis of panel data. *Economica* 55 (218), 284. <https://doi.org/10.2307/2554479>.
- Sobrino, J.A., Jiménez-Muñoz, J.C., Soria, G., Ruescas, A.B., Danne, O., Brockmann, C., Ghent, D., Remedios, J., North, P., Merchant, C., Berger, M., Mathieu, P.P., Götsche, F.M., 2016. Synergistic use of MERIS and AATSR as a proxy for estimating land surface temperature from sentinel-3 data. *Rem. Sens. Environ.* 179, 149–161. <https://doi.org/10.1016/j.rse.2016.03.035>.
- Sohrabi, C., Alsafi, Z., O'Neill, N., Khan, M., Kerwan, A., Al-Jabir, A., Iosifidis, C., Agha, R., 2020. World Health Organization declares global emergency: a review of the 2019 novel coronavirus (COVID-19). *Int. J. Surg.* 76 (February), 71–76. <https://doi.org/10.1016/j.ijisu.2020.02.034>.
- Song, J., Lin, T., Li, X., Prishchepov, A.V., 2018. Mapping urban functional zones by integrating very high spatial resolution remote sensing imagery and points of interest: a case study of Xiamen, China. *Rem. Sens.* 10 (11). <https://doi.org/10.3390/rs10111737>.
- Srivastava, P.K., Majumdar, T.J., Bhattacharya, A.K., 2009. Surface temperature estimation in Singhbhum Shear Zone of India using Landsat-7 ETM+ thermal infrared data. *Adv. Space Res.* 43 (10), 1563–1574. <https://doi.org/10.1016/j.asr.2009.01.023>.

- Srivastava, A.K., Bhoyer, P.D., Kanawade, V.P., Devara, P.C.S., Thomas, A., Soni, V.K., 2021. Improved air quality during COVID-19 at an urban megacity over the Indo-Gangetic Basin: from stringent to relaxed lockdown phases. *Urban Clim.* 36 (September 2020), 100791. <https://doi.org/10.1016/j.ul clim.2021.100791>.
- Tan, M., Li, X., 2015. Quantifying the effects of settlement size on urban heat islands in fairly uniform geographic areas. *Habitat Int.* 49, 100–106. <https://doi.org/10.1016/j.habitatint.2015.05.013>.
- Teufel, B., Sushama, L., Poitras, V., Dukhan, T., Bélair, S., Miranda-Moreno, L., Sun, L., Sasmito, A.P., Bitsuamlak, G., 2021. Impact of COVID-19-related traffic slowdown on urban heat characteristics. *Atmosphere* 12 (2). <https://doi.org/10.3390/atmos12020243>.
- Toro, R., Catalán, F., Urdanivia, F.R., Rojas, J.P., Manzano, C.A., Seguel, R., Gallardo, L., Osses, M., Pantoja, N., Leiva-Guzman, M.A., 2021. Air Pollution and COVID-19 Lockdown in a Large South American City: Santiago Metropolitan Area, Chile, vol. 36. *Urban Climate October 2020* <https://doi.org/10.1016/j.ul clim.2021.100803>.
- Venter, Z.S., Brousse, O., Esau, I., Meier, F., 2020. Hyperlocal mapping of urban air temperature using remote sensing and crowdsourced weather data. *Rem. Sens. Environ.* 242 (March), 111791. <https://doi.org/10.1016/j.rse.2020.111791>.
- Walawender, J.P., Szymanowski, M., Hajto, M.J., Bokwa, A., 2014. Land surface temperature patterns in the urban agglomeration of Krakow (Poland) derived from landsat-7/ETM+ data. *Pure Appl. Geophys.* 171 (6), 913–940. <https://doi.org/10.1007/s0024-013-0685-7>.
- Wang, J., Ouyang, W., 2017. Attenuating the surface urban heat island within the local thermal zones through land surface modification. *J. Environ. Manag.* 187, 239–252. <https://doi.org/10.1016/j.jenvman.2016.11.059>.
- Wang, K., Jiang, S., Wang, J., Zhou, C., Wang, X., Lee, X., 2017. Journal of geophysical research. *J. Geophys. Res. Atmos.* 122 (4449), 2131–2154. <https://doi.org/10.1002/2016JD025304>.
- Ward, K., Lauf, S., Kleinschmit, B., Endlicher, W., 2016. Heat waves and urban heat islands in Europe: a review of relevant drivers. *Sci. Total Environ.* 569 (570), 527–539. <https://doi.org/10.1016/j.scitotenv.2016.06.119>.
- WHO, 2020. WHO coronavirus disease (COVID-19) dashboard [WWWDocument]. URL. <https://covid19.who.int/>. (Accessed 1 June 2021).
- Wu, C., Li, J., Wang, C., Song, C., Chen, Y., Finka, M., La Rosa, D., 2019. Understanding the relationship between urban blue infrastructure and land surface temperature. *Sci. Total Environ.* 694. <https://doi.org/10.1016/j.scitotenv.2019.133742>.
- Xue, J., Anderson, M.C., Gao, F., Hain, C., Sun, L., Yang, Y., Knipper, K.R., Kustas, W.P., Torres-Rua, A., Schull, M., 2020. Sharpening ECOSTRESS and VIIRS land surface temperature using harmonized Landsat-Sentinel surface reflectances. *Rem. Sens. Environ.* 251 (August), 112055. <https://doi.org/10.1016/j.rse.2020.112055>.
- Yang, C., Wang, R., Zhang, S., Ji, C., Fu, X., 2019. Characterizing the hourly variation of urban heat islands in a snowy climate city during summer. *Int. J. Environ. Res. Publ. Health* 16 (14). <https://doi.org/10.3390/ijerph16142467>.
- Yang, C., Yan, F., Zhang, S., 2020. Comparison of land surface and air temperatures for quantifying summer and winter urban heat island in a snow climate city. *J. Environ. Manag.* 265 (March), 110563. <https://doi.org/10.1016/j.jenvman.2020.110563>.
- Yang, J., Zhou, J., Götsche, F.-M., Long, Z., Ma, J., Luo, R., 2020. Investigation and validation of algorithms for estimating land surface temperature from Sentinel-3 SLSTR data. *Int. J. Appl. Earth Obs. Geoinf.* 91 (April), 102136. <https://doi.org/10.1016/j.jag.2020.102136>.
- Yao, R., Wang, L., Huang, X., Zhang, W., Li, J., Niu, Z., 2018. Interannual variations in surface urban heat island intensity and associated drivers in China. *J. Environ. Manag.* 222 (April), 86–94. <https://doi.org/10.1016/j.jenvman.2018.05.024>.
- Ye, G., Lin, H., Chen, L., Wang, S., Zeng, Z., Wang, W., Zhang, S., Rebmann, T., Li, Y., Pan, Z., Yang, Z., Wang, Y., Wang, F., 2020. Environmental contamination of SARS-CoV-2 in healthcare premises. *J. Infect.* xxxx, 2–6. <https://doi.org/10.1016/j.jinf.2020.04.034>.
- Zhao, F., Liu, C., Cai, Z., Liu, X., Bak, J., Kim, J., Hu, Q., Xia, C., 2020. Ozone Profile Retrievals from TROPOMI: Implication for the Variation of Tropospheric Ozone during the Outbreak of COVID-19 in China, vol. 764. *Science of the Total Environment.* <https://doi.org/10.1016/j.scitotenv.2020.142886>.
- Zhou, C., Li, S., Wang, S., 2018. Examining the impacts of urban form on air pollution in developing countries: a case study of China's megacities. *Int. J. Environ. Res. Publ. Health* 15, 165. <https://doi.org/10.3390/ijerph15081565>.
- Zou, Y., Charlesworth, E., Yin, C.Q., Yan, X.L., Deng, X.J., Li, F., 2019. The weekday/weekend ozone differences induced by the emissions change during summer and autumn in Guangzhou, China. *Atmos. Environ.* 199, 114–126. <https://doi.org/10.1016/j.atmosev.2018.11.019>.